

Virtual Fragment Screening: Discovery of Histamine H₃ Receptor Ligands Using Ligand-Based and Protein-Based Molecular Fingerprints

Francesco Sirci,[†] Enade P. Istyastono,^{‡,§} Henry F. Vischer,[‡] Albert J. Kooistra,[‡] Saskia Nijmeijer,[‡] Martien Kuijer,[‡] Maikel Wijtmans,[‡] Raimund Mannhold,^{||} Rob Leurs,[‡] Iwan J. P. de Esch,[‡] and Chris de Graaf^{*,‡}

[†]Laboratory for Chemometrics and Chemoinformatics, Chemistry Department, University of Perugia, Via Elce di Sotto, 10, I-06123 Perugia Italy

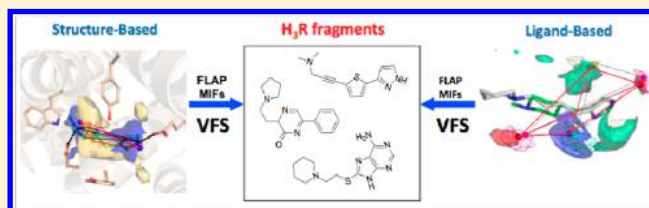
[‡]Division of Medicinal Chemistry, Faculty of Sciences, Amsterdam Institute for Molecules, Medicines and Systems (AIMMS), VU University Amsterdam, De Boelelaan 1083, 1081 HV Amsterdam, The Netherlands.

[§]Molecular Modeling Division, Pharmaceutical Technology Laboratory, Universitas Sanata Dharma, Yogyakarta, Indonesia

^{||}Department of Laser Medicine, Molecular Drug Research Group, Heinrich-Heine-Universität, Universitätsstrasse 1, D-40225 Düsseldorf, Germany

Supporting Information

ABSTRACT: Virtual fragment screening (VFS) is a promising new method that uses computer models to identify small, fragment-like biologically active molecules as useful starting points for fragment-based drug discovery (FBDD). Training sets of true active and inactive fragment-like molecules to construct and validate target customized VFS methods are however lacking. We have for the first time explored the possibilities and challenges of VFS using *molecular fingerprints* derived from a unique set of fragment affinity data for the histamine H₃ receptor (H₃R), a pharmaceutically relevant G protein-coupled receptor (GPCR). Optimized FLAP (Fingerprints of Ligands and Proteins) models containing essential molecular interaction fields that discriminate known H₃R binders from inactive molecules were successfully used for the identification of new H₃R ligands. Prospective virtual screening of 156 090 molecules yielded a high hit rate of 62% (18 of the 29 tested) experimentally confirmed novel fragment-like H₃R ligands that offer new potential starting points for the design of H₃R targeting drugs. The first construction and application of customized FLAP models for the discovery of fragment-like biologically active molecules demonstrates that VFS is an efficient way to explore protein–fragment interaction space *in silico*.



■ INTRODUCTION

Fragment-based drug discovery (FBDD) is a new paradigm in drug discovery that uses small molecules (number of heavy atoms ≤ 22)^{1–4} as starting points for hit optimization.⁵ Fragment-based screening (FBS) is a more efficient way to explore chemical space and generally yields higher hit rates than classical high-throughput screening (HTS) campaigns of drug-like compounds.^{6–8} *Virtual fragment screening* (VFS), the *in silico* prediction of fragment binding to protein targets, has the potential to explore protein–ligand space even more extensively.⁹ Moreover, the computational prediction of protein–ligand interactions and ligand binding orientations by for example molecular docking simulations¹⁰ can be used to efficiently guide the optimization of experimentally validated fragment-like hits and to design target-specific fragment libraries.^{11–15}

Although there are interesting examples of successful VFS studies,^{16,17} most VS studies, and particularly those focusing on G protein-coupled receptors (GPCRs), have mainly focused on

the identification of larger ligands.¹⁸ While the recent crystal structure determinations of various class A GPCRs¹⁹ has opened up opportunities in structure-based ligand discovery for this pharmaceutically important protein family, there are still several other unresolved challenges in VFS. For *structure-based* VS techniques, including molecular docking and structure-based pharmacophore screening, there are problems concerning sampling and scoring of different protein–ligand configurations.^{7,20} Small fragments can adopt a larger variety of binding modes in different protein (sub)pockets, making structure-based VS more sensitive to binding site definition and (essential) pharmacophore feature identification, and dependent on the performance of the conformational sampling algorithm used. In addition, scoring functions used to estimate the binding affinity and determine binding modes in molecular docking are not trained for ranking (the poses of) small

Received: August 28, 2012

Published: November 9, 2012

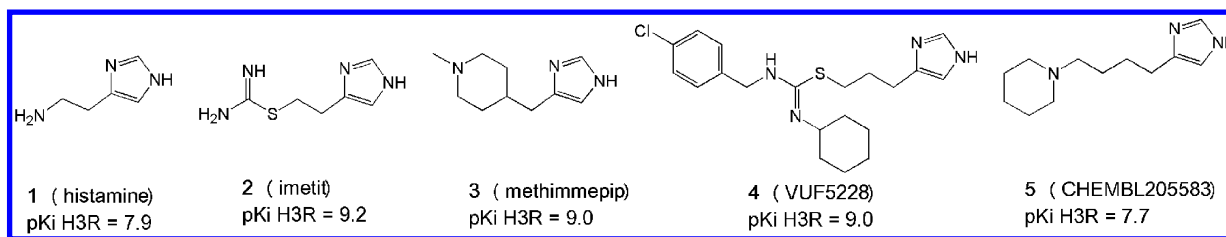


Figure 1. Molecular structure of H₃R ligands 1–5. Ligand affinity data (pK_i values) are from refs 64,71,107, and 108.

fragment-like compounds.^{13,21,22} In *ligand-based* VS for fragment-like molecules there are challenges concerning size dependence of topology-, pharmacophore-, and shape-based similarity. Chemical similarity measure cutoffs are shown to be strongly molecular size dependent.^{23,24} Furthermore, when only disconnected groups (maximum common edge subgraph MCE)²⁵ are common in ligands, shape/pharmacophore-based methods have difficulties in identifying chemical similarity.²⁶ In addition to the technical challenges of both ligand- and structure-based VS methods, there is a lack of proper training and test sets to validate and optimize VFS approaches. First of all, many protein targets have relatively low affinities for small fragments and therefore the number of known active fragment-like molecules to construct predictive *in silico* models is often relatively low. Second, although target annotated ligand libraries^{27–30} are useful sources for compiling challenging training and test sets of known actives, the number of true *inactives* in these databases (and particularly the number of inactive fragments) is very low. As an alternative, focused decoy databases with similar physicochemical properties as known actives has been constructed for retrospective validation experiments.³¹ However, assumed true negatives may actually be positives in reality.³²

In the present study, we aim to address the different challenges in virtual fragment screening by a systematic comparison of different ligand-based and structure-based *in silico* methods in their ability to (i) discriminate active from inactive fragment-like molecules in *retrospective* validation studies and (ii) identify new fragment-like ligands in *prospective* virtual screening runs. For this purpose we used a unique training set of in-house screening data of a chemically diverse library of fragment-like molecules⁴ against the histamine H₃ receptor (H₃R), a receptor involved in many neurological processes.^{33,34} H₃R can bind fragment-like compounds (e.g., histamine (1), imetit (2), and methimempip (3), see Figure 1) with high affinity.³⁵ We compared the retrospective virtual screening accuracy of the novel fingerprint-based VS method FLAP (fingerprint for ligands and proteins)^{36–40} to topological fingerprint-based (extended connectivity fingerprint, max distance 4; ECFP-4)⁴¹ and shape-based (rapid overlay of chemical structures; ROCS)⁴² chemical similarity methods as well as protein-based docking approaches (PLANTS and GOLD).^{43,44} In the FLAP method, four-point pharmacophores, derived from molecular interaction fields (MIFs), based on H (shape), DRY (hydrophobic), N1 (H-bond acceptor), and O (H-bond donor) GRID interaction probes, are used to align molecules with specific biological activity. Linear discriminant analysis (LDA) is then used to identify a representative reference ligand for the alignment of molecules and derive a linear combination of probe scores that is capable of discriminating molecules with different biological activity.^{38,45,46}

In the current study the FLAP method was shown to be particularly suitable to overcome challenges in VFS related to

conformational sampling, shape similarity, and the identification of *essential* interaction features for ligands and proteins. This FLAP approach was successfully used to identify new fragment-like H₃R ligands in prospective virtual screening studies. Our comparative and prospective study of different VFS approaches identifies several challenges in the *in silico* prediction of fragment binding. The successful application of customized FLAP models, however, demonstrates that VFS is indeed an efficient way to explore protein-fragment space *in silico*.

METHODS

Training and Test Set Selection for Retrospective VS.

For training and validation of ligand- and structure-based FLAP models, a data set has been created from two sources. Part of the actives was selected from the ChEMBL database using a $pK_i > 7.0$ as an affinity cutoff. The remaining actives and inactives stem from the VU-MedChem fragment library,⁴ including 60 actives ($\geq 50\%$ radioligand displacement from H₃R at 10 μ M) and 871 inactives ($\leq 30\%$ radioligand displacement, Supporting Figure S1). This data set, containing 1202 molecules, was divided by random selection into two distinct training sets and two test sets named training set 1, training set 2, test set 1, and test set 2 (Figure 2A) for independent model generation and retrospective virtual screening evaluation studies (Figure 2B) in order to evaluate the robustness of the FLAP models and to avoid topology-, pharmacophore-, and shape-based similarity dependent performance of the different virtual screening methods.^{23–26} The FLAP method requires training sets with approximately the same number of active and inactive molecules.⁴⁷ The remaining compounds were collected for test set generation, without biased exclusion of ligands. Both the training and test sets contain molecules with similar physicochemical properties (Supporting Information Figure S3A–B; Table S4). Conformers were generated with CORINA v.3.46⁴⁸ for each compound. Microspecies were also generated with FLAP internal tools: Tauthor v.1.4.90 and Blabber v.1.4.90 which are part of the MoKa package.⁴⁹ Finally, FILTER (OpenEye)⁵⁰ was used to select compounds having at least one basic charged group.

Database Preprocessing. OpenEye's FILTER⁵⁰ was used to filter the fragment-like training and test sets using the following criteria: number of heavy atoms, ≤ 22 ; number of rotatable bonds, ≤ 5 ; number of H-bond acceptors, ≤ 3 ; number of H-bond donors, ≤ 3 (see also Supporting Information Figure S5). A further filtering criterion was to select only charged compounds. CORINA v.3.46 was used to generate 3D minimized structures for all retrospective data sets. The original stereoisomeric configurations of ligands were retained. The MoKa algorithm⁴⁹ in FLAP was used to calculate all possible microspecies for each ligand. For each data set, all possible protomeric and tautomeric microspecies were generated,

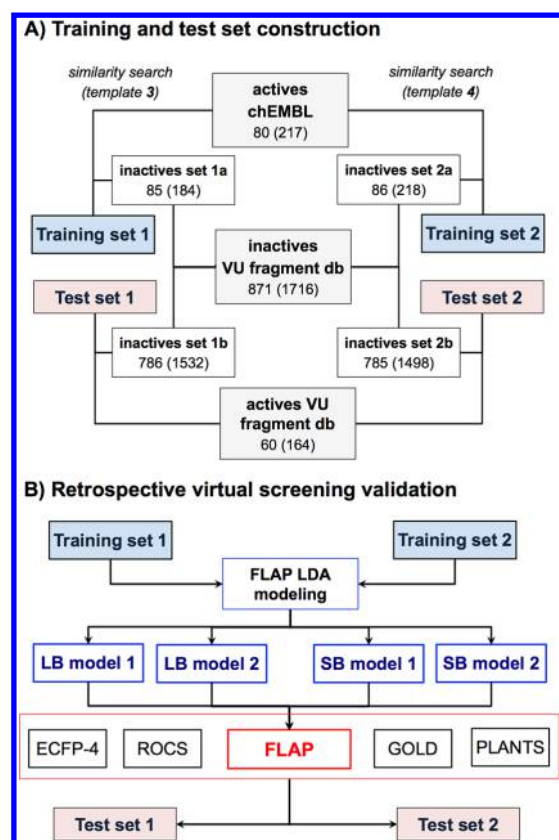


Figure 2. Workflows of (A) the construction of training and test sets containing molecules with affinity data (active or inactive) for H₃R extracted from the ChEMBL database^{28,95} and the VU-MedChem fragment library⁴ for (B) development and validation of ligand-based (LB) and protein structure-based (SB) FLAP models and other ligand-based (ECFP-4,⁴¹ ROCS⁴²) and structure-based (GOLD,⁴³ PLANTS⁴⁴) virtual screening methods.

discarding those with a predicted abundance <1%. Stereoisomeric forms were also calculated.

Construction and Validation of FLAP Models. FLAP and Linear Discriminant Analysis (LDA). The software FLAP³⁶ was used to build, validate, and perform retrospective and prospective ligand-based and structure-based virtual screening for histamine H₃R ligands. FLAP was successfully applied in previous medicinal chemistry projects for ligand-based and structure-based virtual screening, pharmacophoric hypothesis generation, and comparison of protein–ligand binding sites.^{38–40,51,52} It is based on GRID force-fields³⁷ in order to evaluate type, strength, and direction of the interactions a molecule can have. LDA (linear discriminant analysis)^{45,46} was used to train FLAP models. LDA is implemented in FLAP and can be used to select templates and probe scores on the basis of how they are capable to generate descriptive models which discriminate experimentally active from inactive molecules.

FLAP considers the template molecule(s) as fixed, with the query molecules being oriented onto them. Thus, each template functions as a generator of descriptors; their total number depends both on the number of templates used and the number of probes. The output of an LDA analysis is a continuous descriptor named LDA-R that estimates the classification of a ligand as active or inactive. Since each template is a generator of descriptors, it will produce a different classification of the calibration set molecules, with varying

accuracy. Each template therefore exhibits an individual performance, in the sense that each template can generate descriptors that are better or worse in separating the active and inactive molecules into their respective classes.

The LDA tool was applied to build ligand- and structure-based models. For ligand-based model generation, one template was selected and a set of three scores that best discriminate active from inactive molecules for training sets 1 and 2. For structure-based model generation, three of the four templates were selected and a set of four scores that best discriminate active from inactive molecules for training sets 1 and 2. In this approach, the templates are represented by the binding site of the histamine H₃R homology model generated from H₁ crystal structure as template (PDB code: 3RZE).⁵³

GRID Probes. FLAP databases for retrospective and prospective VS were generated using the GRID probes H, DRY, N1, and O with a spatial resolution of 0.75 Å. For each ligand, up to 25 conformers were generated (with an RMSD cutoff of 0.3 Å between two conformers). The H probe describes the shape of the molecular target (i.e., ligand and protein in ligand-based and structure-based FLAP models, respectively), whereas the DRY probe detects aromatic and hydrophobic interactions. The hydrogen-bond acceptor and hydrogen-bond donor capacities of the target are described by the amide N1 probe (similar to N1=, NH=, N2, N2=, N3+, N2+, and O1 GRID probes) and carbonyl O probe (similar to O=, O::, and O= probes), respectively.

FLAP Docking and FLAP VS. The Flapsite tool was used to generate the cavities for all the molecular dynamic snapshot complexes of H₃R–3, with a spatial GRID resolution of 1.0 Å. A pocket point radius of 2.0 Å was considered as input for the computation of structure-based LDA models. Finally, N1 acceptor field of D114^{3,32} was defined as an essential interaction in the FLAP models, because this conserved residue in bioaminergic receptors⁵⁴ is shown to be essential in histamine receptor binding.^{55–58} FLAP LDA-R and Glob-sum were used for ranking actives and inactives in retrospective and prospective virtual screening studies.

ECFP-4 2D Similarity Search. Two-dimensional similarity searches were carried out using ECFP-4 (extended connectivity fingerprints)⁴¹ descriptors available in Accelrys Scitegic Pipeline Pilot⁵⁹ and compared using the Tanimoto coefficient.

ROCS 3D Shape-Based Similarity Search. The conformer database was generated using standard settings OMEGA⁶⁰ and searched with ROCS⁴² using standard settings as well. The conformations of reference H₃R ligand 1 was used as query molecules for independent ROCS⁶¹ runs. Compounds were ranked by decreasing Comboscore⁶¹ (combination of shape Tanimoto and the normalized color score in this optimized overlay).

Correlation Distance Index. The Pearson's distance coefficient (*R*) was used for correlating FLAP vs ROCS vs ECFP-4 scores.⁶² Pearson's distance has been reported as a standard measure of the correlation between two variables *X* and *Y*, calculated as

$$R = 1 - \frac{\sum_{i=1}^n (X_i - \bar{X}_i)(Y_i - \bar{Y}_i)}{\sqrt{\sum_{i=1}^n (X_i - \bar{X}_i)^2} \sqrt{\sum_{i=1}^n (Y_i - \bar{Y}_i)^2}}$$

Analysis Retrospective Virtual Screening Studies.

Virtual screening accuracies were determined in terms of area under the curve of receiver–operator characteristics (ROCs, with 95% confidence interval) and enrichment *E* in true

positives (TP) at different false positive rates (FP_x): $E = TP / FP_x$.⁶³ Early enrichments at 0.5%, 1%, 2%, and 5% FP rates were computed for each virtual screening as calculated as recommended by Jain and Nicholls.⁶³

Construction and Refinement of H₃R Homology Models. An initial H₃R model was constructed based on the H₁R crystal structure⁵³ with MODELLER (using the same protocol as previously published for H₄R⁶⁴) and refined by docking and molecular dynamics simulations with H₃R ligands 3 and 4. For each H₃R-ligand complex, optimal structures were selected based on their ability to discriminate between known fragment-like H₃R ligands and true fragment-like H₃R inactives in retrospective virtual screening studies (Supporting Information Figure S6). The reference compounds 3 and 4 were docked into the H₄R binding pocket using PLANTS version 1.1.⁴³ The best ranked poses of 3 and 4 forming H-bond interactions to D114^{3,32} and E206^{5,46} (residues proposed to be involved in ligand binding in histamine H₃/H₄ receptors)^{57,58,64,65} were selected and minimized using AMBER 10⁶⁶ to relax the structure. Force-field parameters for the ligands were derived using the Antechamber program,⁶⁷ and partial charges for the ligands were computed using the AM1-BCC procedure in Antechamber. Upper-bound distance restraint of 3.5 Å to maintain the interaction of the ligand to D114^{3,32} was applied. The minimized model was subsequently embedded in a pre-equilibrated lipid bilayer consisting of molecules of 1-palmitoyl-2-oleoylphosphatidylcholine (POPC) and solvated with TIP3P water molecules as described by Urizar et al.⁶⁸ The complexes embedded in the hydrated lipid bilayer were minimized shortly using AMBER 10. The hydrogen bond to D114^{3,32} constraint and a positional harmonic constraint of 50 kcal/mol·Å on Cα carbon atoms were applied. The entire system was then subjected to a 1.1 ns constant pressure molecular dynamics (MD) simulation. All bonds involving hydrogen atoms were frozen with the SHAKE algorithm. During the first 100 ps, the Cα carbon atoms were constrained, the hydrogen bond of the ligand to D114^{3,32} was restrained as previously described, and the temperature was linearly increased from 0 to 300 K. During the last 1000 ps, the temperature was kept constant at 300 K and the pressure at 1 bar, using a coupling constant of 0.2 ps and the Berendsen approach. Interactions were calculated according to the AMBER03 force field, using particle-mesh-ewald (PME) summation to include the long-range electrostatic forces. van der Waals interactions were calculated using a cutoff of 8.0 Å. MD snapshots were clustered with the GROMACS g_cluster tool with respect to the Cα atoms of the defined binding residues and according to the Jarvis–Patrick method,⁶⁹ using a cutoff of 3 Å for defining the nearest neighbors. This yielded four clusters per simulation run. The MD snapshots of the complexes were finally energy minimized as described before. The minimized ligand–protein complexes from the MD snapshots were subjected to retrospective virtual screening studies.

Selection of H₃R–Ligand Complexes by Retrospective Structure-Based Virtual Screening. Representative minimized MD snapshots of H₃R–3 and H₃R–4 complexes were evaluated in retrospective virtual screening studies of the H₃R training and test sets (Figure 2A) using PLANTS⁴³ and GOLD⁴⁴ docking programs in combination with a protein–ligand interaction fingerprint (IFP) scoring method (Figure 2C).¹³ Seven different interaction types (negatively charged, positively charged, H-bond acceptor, H-bond donor, aromatic

face-to-edge, aromatic-face-to-face, and hydrophobic interactions) were used to define the IFP between the reference ligand and the following binding site residues: L111^{3,29}, D114^{3,32}, Y115^{3,33}, C118^{3,36}, T119^{3,37}, Y167^{4,58}, E185^{ECL2}, H187^{4,99}, A190^{ECL2}, F192^{ECL2}, F193^{ECL2}, L199^{5,39}, A202^{5,42}, S203^{5,43}, T204^{5,44}, E206^{5,46}, F207^{5,47}, W255^{6,48}, Y258^{6,51}, Y259^{6,52}, M262^{6,55}, Y278^{7,35}, F282^{7,39}. A Tanimoto coefficient (Tc-IFP) measuring IFP similarity with the reference poses of 3 or 4 in the H₃R models was used to score the docking poses of actives and inactives forming a hydrogen bond to D114^{3,32}.^{57,58} Early enrichment (EF_{1%}) values derived from receiver operating characteristic (ROC) curves were used as virtual screening criteria to evaluate the applicability of the MD snapshots to discriminate between known fragment-like H₃R ligands and true fragment-like H₃R inactives in retrospective virtual screening studies (Figure 2C). The snapshots yielding the highest retrospective structure-based virtual screening accuracies were used further in prospective virtual screening.

Compounds Selected by Virtual Screening. The compounds selected by virtual screening were purchased from available screening collections of 7 vendors (Supporting Information Table S7): Chembridge (www.Hit2Lead.com), Enamine (www.enamine.com), Vitas-M (www.vitasmlab.com), Life Chemicals (www.lifechemicals.com), ChemDiv (www.chemdiv.com), MayBridge (www.maybridge.com), and TimTec (www.timtec.com). The purity of all compounds was verified by liquid chromatography–mass spectrometry (LCMS), and all 18 experimentally validated hits had a purity of 95% or higher (Supporting Information Table S8).

Cell Culture, Transfection, and Membrane Preparation. The displacement binding assays were performed using homogenized transfected cells in 50 mM Tris-HCl binding buffer (pH 7.4 at room temperature (RT)). These cell homogenates were coincubated with 10 μM of the compounds and ~10 nM [³H]-pyrilamine (hH₁R), ~1 nM [³H]-N-α-methylhistamine (NAMH) (hH₃R), or ~10 nM [³H]-histamine (hH₄R) in a total volume of 100 mL/well. The reaction suspensions were incubated for 1.5 h at RT on a shaking table (750 rpm). A bound radioligand was separated from the free radioligand via rapid filtration over a 0.5% PEI-pres soaked glass fiber C plate (GF/C, Perkin-Elmer). GF/C plates were subsequently washed three times with ice-cold 50 mM Tris-HCl wash buffer (pH 7.4 at 4 °C). The retained radioactivity on the GF/C plates was counted by liquid scintillation counting in a Wallac Microbeta (Perkin-Elmer). [³H]-Pyrilamine (25.8 Ci/mmol), [³H]-N-α-methylhistamine (85.0 Ci/mmol), and [³H]-histamine (13.4 Ci/mmol) were purchased from Perkin-Elmer. Nonlinear curve fitting was performed using GraphPad Prism 5.0d software. The K_i values were calculated using the Cheng–Prusoff equation $K_i = IC_{50} / (1 + [radioligand] / K_d)$.⁷⁰

■ RESULTS

Training and test sets were used to build (Figure 2B, Figure 3) and retrospectively validate (Figures 3–6, Tables 1–3) ligand-based and structure-based virtual screening methods. Validated FLAP models were finally applied in prospective virtual screening studies to identify new H₃R ligands (Figures 7–10, Table 4).

Retrospective Validation of Ligand-Based FLAP Models. Four-point pharmacophores derived from molecular interaction fields (MIFs), based on H (shape), DRY (hydrophobic), N1 (H-bond acceptor), and O (H-bond donor) GRID interaction probes were used to align known H₃R molecules

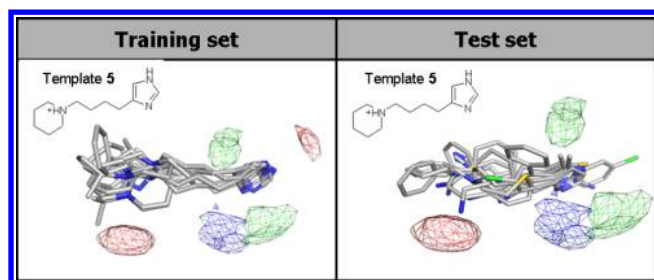


Figure 3. Alignment of data set molecules onto template 5 is shown. For 3D MIF analysis, donor interaction regions are given in red, acceptor interaction regions, in blue, and hydrophobic interaction regions, in green. The red donor region generated by the basic protonated moiety plays the most important role in this ligand-based analysis.

from the training sets (Figure 2). It should be noted that the use of other probes (e.g., the hydrophobic C1= probe instead of or combined with the aromatic/hydrophobic DRY probe) would give other four-point pharmacophores. The pragmatic choice for these four specific probes is however justified by the fact that they represent distinct ligand–protein interaction features but keep the amount of variables (similarity scores for each probe and their combinations) manageable. Linear discriminant analysis (LDA)^{45,46} of the overlap of the MIFs of the aligned molecules identified compound 5 (ChEMBL205583,⁷¹ Figure 1) as the best template for the construction of two different ligand-based FLAP models (Figure 3): LB model 1 (based on training set 1, consisting of 2 H-bond donors, 1 H-bond acceptor, and 2 DRY MIFs) and LB model 2 (based on training set 2, consisting of 1 H-bond donor, 1 H-bond acceptor, and 2 DRY MIFs). The LDA analysis furthermore indicated that the microspecies with the basic protonated piperazine and the neutral imidazole moiety was optimal for the discrimination between known fragment-like H₃R ligands and inactive fragments.

LB models 1 and 2 were able to efficiently discriminate known H₃R ligands from inactive molecules in retrospective virtual screening studies (Table 1 and Figure 4), indicated by a high global virtual accuracy (AUROC values of 0.86 and higher) and early enrichment factors⁶³ (enrichments of 22 and higher at 1% false positive (FP) rates) for both training and test

sets. The virtual screening accuracies of FLAP models were comparable to or significantly better than the *in silico* screening accuracies of two other ligand-based screening methods, the topological circular fingerprint-based method ECFP-4,⁴¹ and the shape and pharmacophore similarity based method ROCS⁴² (Table 1, Figure 4). Both FLAP models performed equally well in discriminating active H₃R ligands from inactive molecules in the test set, indicating that both ligand-based models are robust (Table 1, Figure 4). In particular LB model 2 had a superior virtual screening performance for the training set (Table 1). We therefore decided to select LB model 2 for prospective virtual screening. It should be noted that LDA models based on the simultaneous use of different templates did not yield better results than the use of a single template (data not shown). Apparently the identification of essential and conserved molecular hotspots by the FLAP method based on a single reference ligand structure is sufficient for the H₃R protein target. Furthermore FLAP automatically selects the tautomeric, protomeric, or stereoisomeric form of a ligand that best fits the models. Most of the selected candidate microspecies have a neutral imidazole and a basic protonated moiety.

For 3D GRID MIFs analysis, the 20 top-ranked training and test set compounds were superimposed onto the template 5 (Figure 3). The alignments were generated according to the highest Glob-sum score solution for each screened candidate. Glob-sum is a global similarity score calculated by summing the H, N1, DRY, and O descriptors. Taking into account the most relevant molecular interaction fields shared among a set of aligned molecules, MIF cumulative analysis revealed the important role of both the large donor region generated by the basic protonated moiety as well as the interaction fields that correspond to the neutral form of the imidazole moiety in template 5 (see also the Discussion section).

Comparison of Ligand-Based VFS Methods: FLAP versus ECFP-4 and ROCS. Results of retrospective ligand-based modeling with FLAP were compared with results using the 2D similarity search method ECFP-4⁴¹ and the 3D similarity search method ROCS.⁴² The latter two methods are selected as representative complementary virtual screening methods that have been extensively used in previous comparative VS studies.^{72–77} We used the Tanimoto similarity coefficient for consistent comparison of all ligand-based virtual

Table 1. Enrichment Factors of Ligand-Based FLAP Models vs EFs from ECFP-4 and ROCS^a

		LB model 1				LB model 2			
		FLAP Glob-sum	FLAP LDA-R	ECFP-4	ROCS	FLAP Glob-sum	FLAP LDA-R	ECFP-4	ROCS
training set	EF 0.5%	72.5	45	49.6	28.7	122.5	117.5	70.3	42.1
	EF 1%	36.3	22.5	24.8	18.4	61.3	58.8	35.1	21.0
	EF 2%	23.1	26.3	17.2	13.2	32.5	30	19.6	12.8
	EF 5%	15	16	9.5	7.6	14.3	16.3	9.1	7.1
	AUC	0.95	0.91	0.79	0.81	0.91	0.93	0.72	0.74
	(interval)	0.91–0.98	0.91–0.98	0.73–0.85	0.77–0.85	0.86–0.96	0.87–0.99	0.69–0.75	0.71–0.77
test set	EF 0.5%	53.1	43.3	28.3	18.3	50	34.4	26.9	17.8
	EF 1%	26.6	30	19.5	12.2	26.6	26.6	19.0	12.1
	EF 2%	17.2	18.3	12.4	8.6	17.2	17.2	12.8	8.8
	EF 5%	9.1	11.3	6.8	5.6	9.1	10.6	7.0	5.7
	AUC	0.86	0.86	0.74	0.8	0.86	0.87	0.74	0.8
	(interval)	0.81–0.91	0.81–0.92	0.68–0.80	0.75–0.85	0.81–0.91	0.81–0.92	0.68–0.80	0.75–0.85

^aEnrichment factors (EF) for ligand-based FLAP models are compared with the EFs from ECFP-4 and ROCS screening studies. AUC denotes the area under the ROC curve. EF_{0.5}, EF₁, EF₂, EF₅, and AUC_{max} correspond to the enrichment factors at 0.5%, 1%, 2%, and 5% of the false positives in logarithmic scale.

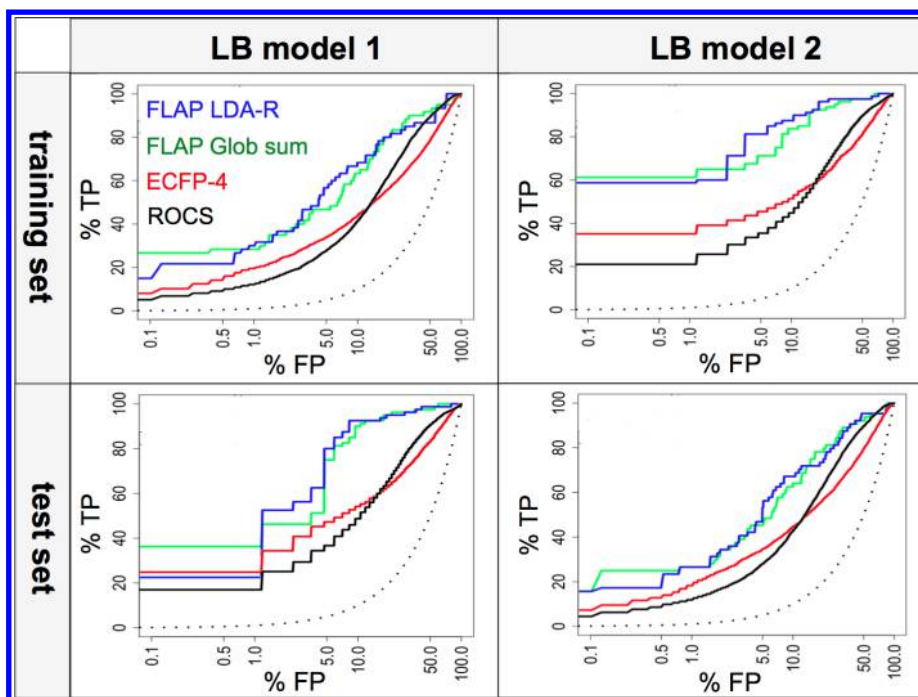


Figure 4. Enrichment curves of retrospective ligand-based virtual screening studies to discriminate known H₃R ligands (true positives, TP) from molecules that have no affinity for H₃R (false positives, FP) in different training and test sets (Figure 1A), using FLAP Glob-sum (green), FLAP LDA-R (blue), ECFP-4 (red), and ROCS (black). Glob-sum is a global similarity score calculated by summing the H, N1, DRY, and O descriptors. LDA-R estimates the probability of predicting a screened candidate either as active or inactive.

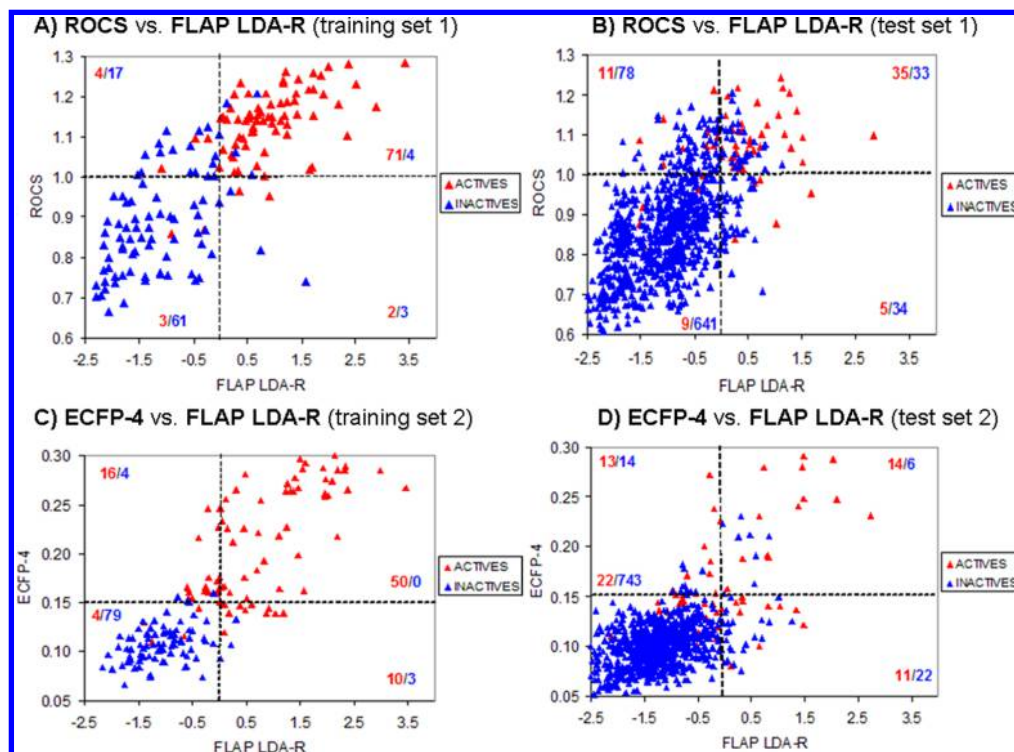


Figure 5. Scatter plot comparison of FLAP LDA-R versus ECFP4 and ROCS. The dashed lines indicate the discrimination between actives and inactives. The number of actives and inactives in each quadrant are indicated in red and blue, respectively.

screening methods, as the Tanimoto index is the standard similarity metric for the comparison of FLAP MIFs³⁶ and ROCS shape and pharmacophore similarity.⁴²

We first evaluated the potential different contributions that each microspecies of the candidates and the templates might

give.^{49,78–85} For consistency with the FLAP procedure, we selected the specific microspecies for each candidate that corresponds with the template structure (compound **5** which contains a basic protonated piperidine ring and a neutral imidazole moiety) and analyzed four different cases for

microspecies selection (Supporting Information Figure S2). After generating the similarity matrices for each case, the final enrichment curve was calculated by averaging all the single similarity values calculated against each template. Since very similar results were obtained (data not shown) from the different microspecies cases, only enrichment curves for *case 4* are shown in Figure 4 (see also Supporting Information Figure S2-C1-C4). FLAP models give significantly higher retrospective VS accuracies than ECFP-4 and ROCS (Table 1, Figure 4) for all compound sets except training set 1 (for which ECFP-4 shows comparable early enrichments as LDA-R).

In addition, we evaluated the possible interdependence of the three similarity methods, by plotting LDA-R scores from FLAP models versus Tanimoto scores from ROCS and ECFP-4 models for both training and test sets (Figure 5). FLAP LDA-R is not a similarity score but instead it is a continuous score generated during LDA calibration that quantifies the probability of a molecule to be predicted as active (positive values) or inactive (negative values); see the Methods section. For ROCS similarity, we used the ComboScore,⁶¹ which combines the Shape Tanimoto score (3D overlapping of shapes) and the Color Score (common pharmacophore features within template and query compounds). No correlation was found (Table 2),

Table 2. Correlation Matrix for the Similarity Methods FLAP/ECFP-4/ROCS^a

	training set 1	test set 1	training set 2	test set 2
ROCS	0.62	0.41	0.59	0.48
ECFP-4	0.62	0.27	0.68	0.34

^aThe R^2 was calculated between the FLAP LDA-R score versus Tc-ROCS and Tc-ECFP-4 for each data set.

indicating that the methods are independent (see the Methods section). Thus they are able to detect different features and molecular properties. In other words, these results demonstrate that the ligand-based FLAP procedure can provide information that is not detectable by the ROCS and ECFP-4 methods.

Retrospective Structure-Based FLAP Models. Two further models were generated applying the structure-based mode of FLAP and using the same data sets described for ligand-based FLAP models. Methimepip (3),⁸⁶ representing a

small high affinity ligand, and VUF5228 (4),^{87,88} representing a somewhat larger one, were docked into a H₃R homology model based on the recently solved crystal structure of the histamine H₁R (3RZE)⁵³ and subjected to molecular dynamics (MD) simulations. For each MD-trajectory of both H₃R complexes four representative snapshots were selected by clustering and subsequently used as templates for structure-based FLAP modeling. Two models were developed: the first, generated from H₃R-3 snapshots, is called SB model 1; the second, generated from H₃R-4 snapshots, is called SB model 2. Different combinations of possible templates were tested and two receptor structures belonging to the H₃R-3 complex (SB model 1) were shown to represent the most predictive and robust model. The H-bond acceptor field (N1 probe) of D114^{3,32} was defined as an essential interaction in both FLAP models as site-directed mutagenesis studies have indicated that this conserved residue forms essential H-bond/ionic interactions with basic protonated nitrogen atoms in ligands of bioaminergic receptors⁵⁴ and histamine receptors in particular.^{55–58} We performed retrospective VS using SB model 1 and SB model 2 for the corresponding training and test sets. Their performance was evaluated using early enrichment curves as suggested by Jain and Nicholls.⁶³ Table 3 and Figure 6 summarize the VS enrichment in term of AUROC values and enrichment values at 0.5%, 1%, 2%, and 5% FP rates.

When not specified, FLAP automatically selects that tautomeric, protomeric, or stereoisomeric form of a ligand that best fits the models. Most of the selected candidate microspecies have a basic protonated moiety. On the other hand, the imidazole moiety is present in the neutral or protonated form without any tendency. This might be due by the possibility of such moiety to interact with E206^{5,46} either with NH of the neutral form or NH⁺ of the charged ring.

Comparison of Structure-Based VFS Methods: FLAP versus PLANTS and GOLD. Results of retrospective structure-based modeling with FLAP were compared with the results using the docking methods PLANTS⁴³ and GOLD.⁴⁴ We also analyzed the possible different contributions of each microspecies of the docked ligands.

To this end, fragment-like H₃R ligands were docked using four different MD snapshots generated with the AMBER⁶⁶ package (see the Methods section). The original ligand pose in

Table 3. Enrichment Factors of Structure-Based FLAP Models vs PLANTS and GOLD Docking^a

		SB model 1			SB model 2		
		FLAP LDA-R	PLANTS	GOLD	FLAP LDA-R	PLANTS	GOLD
training set	EF 0.5%	47.50	45.00	37.50	112.5	43.33	25.00
	EF 1%	23.75	22.50	18.75	56.25	21.67	12.50
	EF 2%	25.62	11.25	9.38	29.38	14.44	10.00
	EF 5%	0.85	6.00	5.50	17.50	8.22	8.50
	AUC	0.89	0.70	0.63	0.98	0.81	0.85
	(interval)	0.85–0.93	0.66–0.75	0.56–0.69	0.96–0.99	0.77–0.85	0.81–0.89
test set	EF 0.5%	32.79	11.43	17.39	0.00	30.77	14.49
	EF 1%	16.39	8.57	8.7	6.06	15.38	7.25
	EF 2%	9.02	4.29	5.8	9.09	8.65	12.32
	EF 5%	5.25	4.00	3.48	6.06	5.77	5.51
	AUC	0.74	0.65	0.69	0.75	0.76	0.78
	(interval)	0.69–0.79	0.60–0.69	0.64–0.73	0.69–0.79	0.71–0.82	0.74–0.82

^aEnrichment factors (EF) of structure-based FLAP models are compared with EFs from PLANTS and GOLD docking studies. AUC denotes the area under the ROC curve. EF_{0.5}, EF₁, EF₂, EF₅, and AUC_{max} correspond to the enrichment factors at 0.5%, 1%, 2%, and 5% of the false positives in logarithmic scale. The table reports only the highest enrichment factors according to single or multiple microspecies.

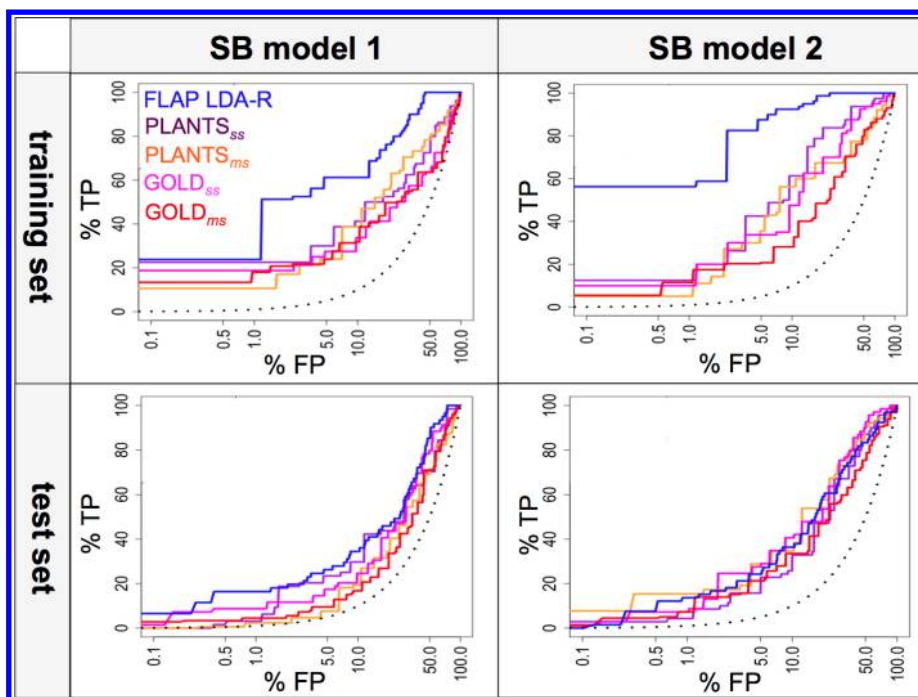


Figure 6. Enrichment curves of retrospective protein structure-based virtual screening studies to discriminate known H₃R ligands (true positives, TP) from molecules that have no affinity for H₃R (false positives, FP) in different training and test sets (Figure 1A), using FLAP LDA-R (blue), PLANTS docking of single species (PLANTS_{ss}, purple), PLANTS docking of multiple species (PLANTS_{ms}, orange), GOLD docking of single species (GOLD_{ss}, magenta), and GOLD docking of multiple species (GOLD_{ms}, red).

the corresponding MD snapshot was used to define reference interaction fingerprints (IFPs) to determine *ligand binding mode similarity* scores of the docking poses of training and test sets (with the reference ligand pose) as described previously.¹³ Only docking poses that donate an H-bond to D114^{3,32} were considered for IFP postprocessing analysis (consistent with the structure-based FLAP procedure). Table 3 lists the best enrichment factors calculated for the four MD clusters. While structure-based FLAP models give significantly better retrospective virtual screening results than docking-based screening with PLANTS and GOLD for training sets 1 and 2 and test set 1, PLANTS docking performs somewhat better than FLAP for test set 2 (Table 3, Figure 6). It should be noted however, that the *training sets* were in fact used to optimize the protein-based FLAP models.

Prospective VS for Fragment-like H₃R Ligands. Starting point for prospective VS was the ZINC database (release 5, 2011)^{89,90} containing roughly 13 million commercially available compounds. This initial collection was filtered using physical–chemical cutoff values close to previously defined fragment-like rules⁴ (number of heavy atoms, ≤ 22 ; number of rotatable bonds, ≤ 5 ; number of H-bond acceptors, ≤ 4 ; number of H-bond donors, ≤ 4 ; Log(P), ≤ 4.0). Compounds containing reactive moieties were also excluded.^{91–93} These combined filters resulted in selection of 156 090 compounds (an overview of the number of molecules that do not obey the “rule of three”⁹⁴ provided in Supporting Information Table S13). These structures were used for the prospective VS using the ligand- and structure-based FLAP models. Figure 7A shows the detailed workflow to extract fragment-like molecules from the ZINC collection of commercially available compounds.

In the next step, we performed prospective VS on the 156 090 zinc compounds using the ligand-based LB model 2 and the structure-based SB model 1. Performance of the latter was

superior to SB model 2 in the above-described retrospective virtual screening study, in particular for the retrieval rate of actives in the test set. Both ligand-based models, however, showed similar performance; LB model 2 was chosen because of its superior virtual screening accuracy for the training set compared to LB model 1.

The FLAP LDA-R score was used for ranking the compounds. A total number of 28973 potential hits had LDA-R scores higher than 0.5 according to the structure-based model (SB model 1) and 1292 potential hits had LDA-R scores higher than 0.5 according to the ligand-based model (SB model 2). The difference in retrieved hit numbers is due to the high MIF similarity that small fragment-like molecules might have with the H₃R binding site. In fact, MIFs of a protein pocket are much more extended than those from a ligand-based approach. The 202 “consensus” hits (with LDA-R scores of 0.5 or higher for both ligand-based and protein-based models) and the top 200 molecules according to the ligand-based model (with structure-based LDA-R scores < 0.5 ; see Figure 7B) were visually inspected with respect to their novelty compared to known scaffolds and their fit in the in-silico models. Eighteen of the 29 hits were experimentally confirmed as H₃R ligands with affinities ranging from 0.5 to 10 μM . Fragments 6, 7, and 8 display (sub)micromolar affinity (K_i values of 0.5, 1.0, and 1.0 μM , respectively; see Table 4 and Figure 8). Only 6 and 13 have affinity for H₁R (K_i values of 0.4 and 1.7 μM , respectively; see Supporting Information Table S9). None of the confirmed H₃R hits have affinity for H₄R.

In order to assess the novelty of the 18 experimentally confirmed H₃R hits, we calculated their ECFP-4 Tanimoto similarity against any known H₃R ligand ($\text{p}K_i \leq 10 \mu\text{M}$) in the ChEMBLdb.⁹⁵ Tanimoto scores for the tested hits range from 0.15 to 0.63, as shown in Table 4.

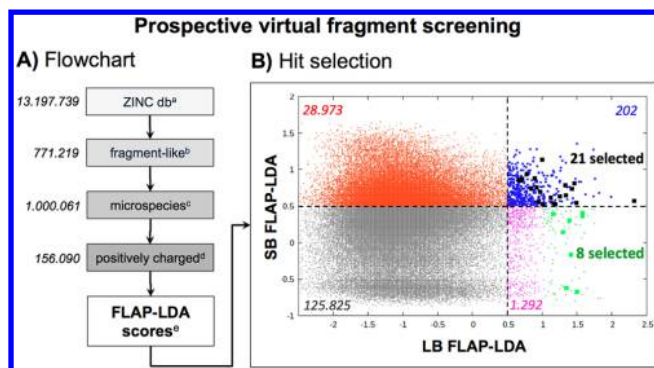


Figure 7. Flowchart of the different steps in prospective virtual screening for new fragment-like H₃R ligands based on ligand-based (LB) and structure-based (SB) FLAP models. (A) Several *in-silico* tools were used to filter the (a) initial collection of commercially available compounds (ZINC)^{89,90} according to (b) fragment-like physicochemical properties close to previously defined fragment-like rules⁴ (number of heavy atoms, ≤ 22 ; number of rotatable bonds, ≤ 5 ; number of H-bond acceptors, ≤ 4 ; number of H-bond donors, ≤ 4 ; Log(P), ≤ 4.0 ; see Supporting Information Table S5) and by exclusion of compounds containing reactive moieties.^{91–93} (c) Microspecies were generated and (d) positively ionized molecules were scored according to ligand-based (LB) and protein structure-based (SB) FLAP models. (B) Individual LB and SB LDA-R FLAP scores (scatter plot) of fragment-like molecules with: (i) LDA-R scores > 0.5 for both ligand-based and protein-based models (consensus hits in blue); (ii) the top 200 molecules according to the ligand-based model with LDA-R score < 0.5 for the protein-based model (green); (iii) LDA-R < 0.5 for the LB model and LDA-R > 0.5 for the SB model, but *not* in the top 200 list of the LB model (orange), (iv) LDA-R > 0.5 for the LB model and LDA-R < 0.5 for the SB model (magenta); (v) LDA-R < 0.5 for both LB and SB models (gray). The experimentally tested consensus hits (21 molecules) top 200 ligand-based hits with SB LDA-R score < 0.5 (8 molecules) are indicated by black and green squares. The dotted lines indicate LB and SB LDA-R cutoff values of 0.5.

None of the experimentally validated hits rank within the top 200 of 2D-based or 3D shape-based similarity searches of the fragment library against using FLAP reference ligand **5** as a template (Table 4). The Tanimoto similarity values of the compounds in the top 200 ranking lists of ECFP-4⁴⁰ and ROCS Comboscore⁴¹ searches range from 0.06 to 0.37 and from 0.68 to 1.51, respectively. Moreover, a combination of previously defined, ECFP-4 (Tanimoto similarity ≥ 0.40)⁹⁶ and ROCS (Comboscore score ≥ 1.40)⁹⁷ cutoffs does not yield any hit (Supporting Information Figure S10). Ligand-based superimposition of the selected hits show an optimal overlap with the MIFs of template **5**, especially for the donor region generated by the probe O (Figure 9, red MIF) complementary to the carboxylate group of D114^{3,32}, a conserved residue in the ligand binding site of bioaminergic receptors⁵⁴ that is shown to be involved in ligand binding to histamine receptors.^{55–58} Our docking simulations suggest that the selected hits form an ionic interaction with the D114^{3,32} and hydrophobic interactions with Y115^{3,33}, Y374^{6,51}, and W402^{7,43} (Figure 10). Residue E205^{5,46} does not make direct ligand interactions in the proposed H₃R–ligand binding mode models. The role of this conserved glutamate residue in H₃R and H₄R has indeed been reported to be ligand dependent in site-directed mutagenesis studies.^{57,58,64,65}

DISCUSSION

The aim of the current study was to investigate the challenges and possibilities of the application of FLAP in fragment-based virtual screening by considering its ability to (i) discriminate active from true inactive fragment-like molecules and (ii) identify new fragment-like ligands for the histamine H₃ receptor. Training and test sets of fragment-like H₃R ligands and true inactive fragment-like molecules, including unique collections of *in-house* H₃R screening data of a chemically diverse library of fragment-like molecules,⁴ were used to build and validate ligand- and structure-based FLAP models. Four-point pharmacophores derived from molecular interaction fields were used to align known H₃R molecules, and linear discriminant analysis was used to identify a representative reference molecule for the alignment and derive a linear combination of probe scores that can discriminate H₃R ligands from inactive molecules. To test their applicability and robustness, the resulting FLAP models were evaluated in retrospective and prospective virtual screening studies and compared to other ligand- and protein-based *in silico* screening methods. The FLAP method was shown to be particularly suitable to overcome challenges in VFS regarding conformational sampling, shape similarity, and the identification of essential interaction features for ligands and proteins.

Challenges of Molecule Size Dependent Ligand-Based VFS. For the ligand-based LB model 1 and LB model 2, the same microspecies of **5** was selected as the template that best discriminates actives from inactives. LDA models based on multiple templates gave similar results compared to the use of a single template. Interestingly, this is the first study in which a FLAP model based on a single template performs as good as FLAP models based on multiple templates.^{98,99}

Ligand-based FLAP models were interpreted using the MIF Cumulative analysis, which considers only those GRID fields that are common for all aligned molecules. In this way, we were able to define the common pharmacophore features of the actives. As expected, the large donor region generated by the basic protonated moiety of the overlapped active fragments plays the most important role in this ligand-based analysis. This conserved ligand H-bond donor moiety is proposed to form an H-bond to the carboxylate moiety of D114^{3,32}, a conserved residue in bioaminergic receptors⁵⁴ that is essential in ligand binding to histamine receptors.^{55–58} Another important feature detected by cumulative analysis regards the neutral imidazole ring, frequently recurring among the superimposed actives from ChEMBL.⁹⁵ This moiety generates three different kinds of MIFs: one acceptor, one donor, and two hydrophobic regions on the top and on the bottom of the imidazole ring. This is expected since those moieties are well overlapping with the template structure.

A challenge of VFS concerns the size dependency of shape-based similarity. Similar retrospective virtual screening accuracies were obtained with LB model 1 and LB model 2 (Figure 4). Although FLAP models have a somewhat better performance for the training sets, all models have consistently high retrospective virtual screening accuracies for both training and test sets (Figure 4). Moreover, optimal FLAP models were successfully applied in prospective *in silico* screening studies to discover new H₃R ligands with a high hit rate of 62%. This confirms the robustness of these models and demonstrates that training sets are not biased by different physicochemical

Table 4. H₃R Binding Affinities and Template Similarities of True Fragment-like Hits

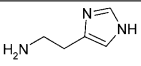
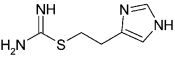
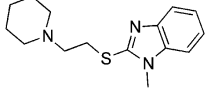
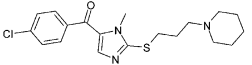
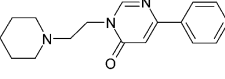
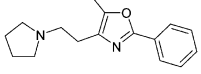
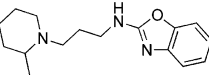
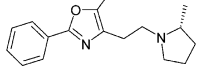
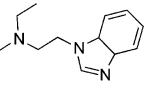
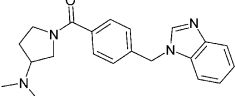
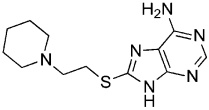
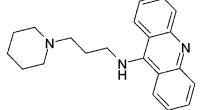
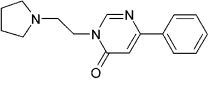
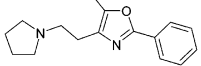
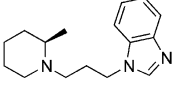
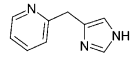
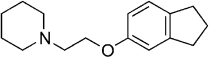
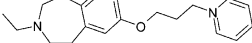
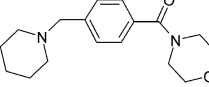
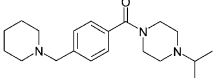
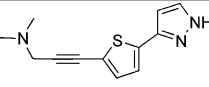
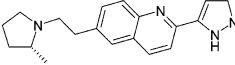
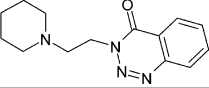
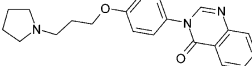
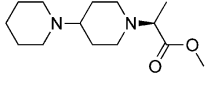
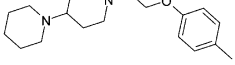
cpd	pK _i ^a	LE ^b	LB LDA-R ^c (rank)	SB LDA-R ^d (rank)	Structure	ROCS ^e cpd 5 (rank)	ECFP-4 ^f cpd 5 (rank)	ECFP4 chEMBL ^g	Closest known H ₃ R ligand ^h
1	7.86±0.04	1.35	1.02 (80) ⁱ	3.72 (1) ⁱ		0.61(87271) ⁱ	0.46(3) ⁱ	-	-
2	9.23±0.04	1.15	0.56 (375) ⁱ	2.21 (2) ⁱ		1.33(210) ⁱ	0.37(19) ⁱ	-	-
6	6.27±0.08	0.45	1.19 (45)	0.52 (197)		1.19 (2796)	0.26 (641)	0.40	
7	6.01±0.01	0.39	1.50 (35)	j		1.01 (16922)	0.26 (635)	0.38	
8	6.00±0.08	0.41	1.58 (22)	j		1.20 (515)	0.19 (4282)	0.40	
9	5.94±0.03	0.51	0.71 (161)	0.87 (87)		0.93 (40255)	0.13 (17613)	0.33	
10	5.88±0.04	0.40	0.97 (94)	0.69 (145)		1.09 (6718)	0.15 (440)	0.30	
11	5.88±0.06	0.42	1.17 (49)	0.53 (193)		0.98 (26432)	0.26 (634)	0.38	
12	5.85±0.10	0.42	1.49 (14)	0.54 (189)		1.24 (1683)	0.23 (1779)	0.44	
13	5.78±0.07	0.44	0.69 (167)	0.85 (93)		1.23 (1068)	0.30 (240)	0.65	
14	5.54±0.08	0.36	1.58 (23)	j		1.07 (12448)	0.20 (3503)	0.65	
15	5.33±0.03	0.39	2.32 (1)	0.57 (176)		1.05 (15582)	0.08 (59809)	0.26	
16	5.35±0.05	0.46	1.35 (66)	j		1.20 (2411)	0.28 (412)	0.44	
17	5.29±0.02	0.40	1.34 (25)	0.64 (157)		1.08 (2875)	0.13 (5432)	0.34	

Table 4. continued

cpd	pK _i ^a	LE ^b	LB LDA-R ^c (rank)	SB LDA-R ^d (rank)	Structure	ROCS ^e cpd 5 (rank)	ECFP-4 ^f cpd 5 (rank)	ECFP4 chEMBL ^g	Closest known H ₃ R ligand ^h
18	5.28±0.06	0.36	0.78 (149)	0.93 (60)		0.99 (29509)	0.083 (59782)	0.33	
19	5.27±0.01	0.36	1.16 (129)	J		1.16 (25678)	0.13 (8629)	0.37	
20	5.17±0.09	0.42	1.41 (52)	J		1.08 (12050)	0.11 (32353)	0.35	
21	5.12±0.11	0.44	0.84 (132)	0.73 (138)		1.11 (10200)	0.10 (37228)	0.19	
22	5.10±0.04	0.35	1.01 (85)	0.52 (198)		1.01 (7860)	0.08 (63082)	0.24	
23	5.01±0.09	0.38	1.46 (16)	0.81 (109)		1.01 (23256)	0.27 (515)	0.33	

^apK_i values are calculated from at least three independent measurements as the mean ± SEM. Values are calculated by displacement of [³H]-methylhistamine binding on membranes of HEK293T cells transiently expressing the hH₃R. ^bLigand Efficiency (LE)⁹⁹ = (ΔG)/N, where the Gibbs free energy of binding ΔG = -RT ln(K_i) and N is the number of non-hydrogen atoms. ^cScore and rank according to FLAP ligand-based LDA score ranking. FLAP LB LDA ranking is given between brackets. ^dScore and rank according to FLAP structure-based LDA score ranking. FLAP SB LDA ranking is given between brackets. ^eROCS 3D shape-based 3D similarity with FLAP selected template 5. ROCS ranking is given between brackets. ^fECFP-4 2D topological similarity with FLAP selected template 5. ECFP-4 ranking is given between brackets. ^gECFP-4 similarity to closest known H₃R actives in ChEMBLdb.⁹⁵ A similarity higher than 0.40 is considered as significant.⁷² ^hClosest known ChEMBL H₃R ligands according to the ECFP-4 fingerprint for each experimentally validated fragment hit. ⁱThe rankings indicated for reference compounds 1 and 2 (histamine and imetit) were determined as if they were included in the screening library ^jProspective hits selected according to the top 200 FLAP ligand-based LDA ranking.

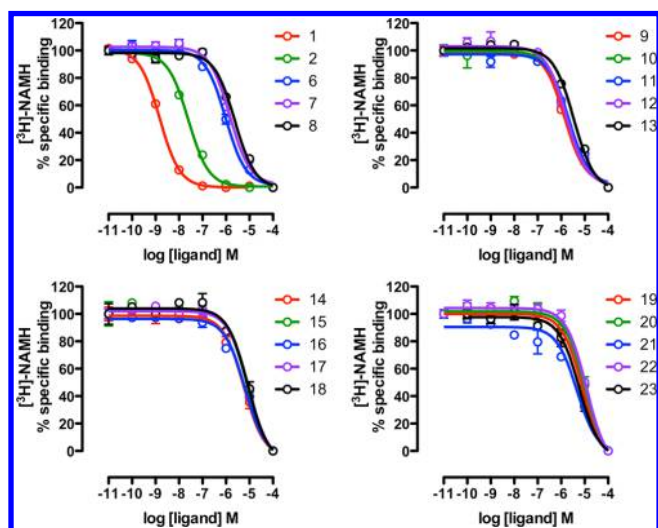


Figure 8. Radioligand displacement of [³H]-methylhistamine by compounds 1–16 in HEK293T cells transiently transfected with human histamine H₃R (*n* = 3, each performed in triplicate).

properties (Supporting Information Figure S3A and B and Table S4).

Overcoming Sampling and Scoring Problems in Structure-Based VFS. Docking-based virtual screening with PLANTS and GOLD gave satisfactory results for both training sets ranking, but FLAP structure-based models perform significantly better for both training sets and test set 1 (Figure 6, Supporting Information Figure S6). PLANTS docking only performs slightly better for test set 2 ranking than the structure-based FLAP models. Molecular docking of fragments can be challenging because of¹² (i) the scoring functions used to estimate and evaluate the binding modes are not trained for fragment-like compounds and (ii) conformational sampling problems of small fragments in large protein binding pockets.^{7,20,21} Recent comparative docking studies showed that there is no significant overall difference between the docking performance of fragment-like molecules and (relatively larger) drug-like molecules²² but indicated that the failure of fragment docking is much more often the result of incorrect *scoring* than of inadequate *sampling* than for drug-like molecules. Docking scoring functions are generally not trained for fragment-like compounds, and poorly estimate solvent

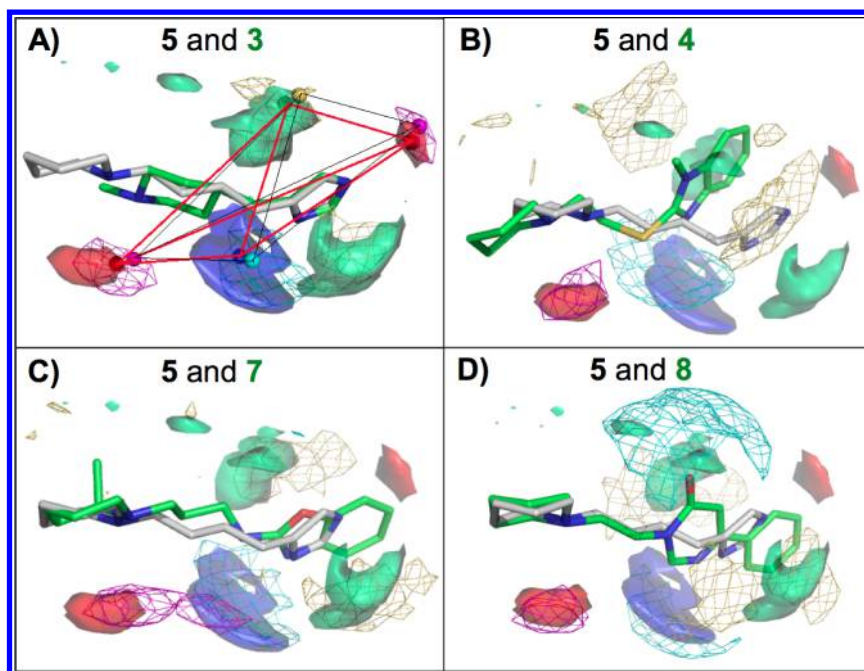


Figure 9. Ligand-based FLAP overlaps of (A) 3 (with hotspots overlaps); (B) 6; (C) 7; and (D) 8 with template 5 (in gray stick). The solid GRID fields represent the MIFs of the template; the GRID fields of the aligned compounds are shown in wireframe. In panel A hotspots quadruplets overlap between template 5 (in red lines) and 3 (in black lines). FLAP superimposition is verified if a pair of quadruplets has all six of their saved distances coupled in a pairwise manner within 1 Å distance of each other, then the quadruplets can be said to give rise to a potentially favorable superposition.

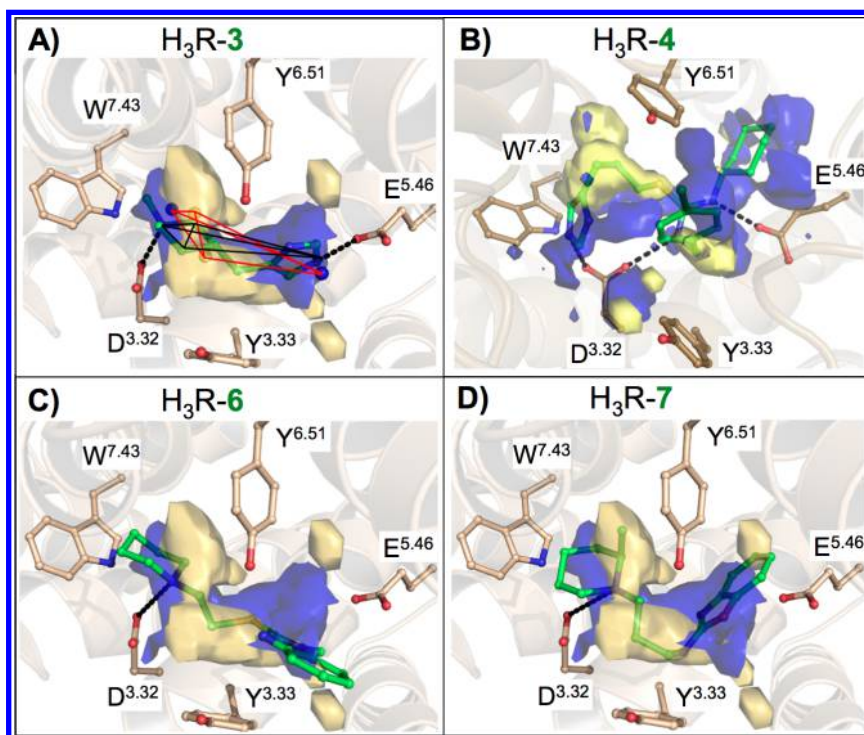


Figure 10. Structure-based FLAP docking pose of 3 (A), 4 (B), 6 (C), and 7 (D) into the H₃R pocket. The blue GRID field indicates two main acceptor regions generated by D114^{3,32} and E206^{5,46}. Hydrophobic regions are shown in yellow. Quadruplet (red lines) of MIF hotspots (spheres) is depicted in panel A. In the structure-based FLAP mode the hotspot quadruplets are extracted from the MIFs of the H₃R pocket. The superimpositions are performed with the same rules as used for the ligand-based mode.

effects and entropic contributions and inaccurately treat long-range effects involved in binding.^{100,101} As a result the scoring accuracy is highly dependent on physicochemical details of target–ligand interactions and fine details of the protein

structure. It is therefore necessary to evaluate different docking–scoring approaches or to optimize scoring functions for training sets before applying them to unknown test cases.¹⁰ Protein–ligand interaction fingerprint (IPF) scoring is an

alternative postprocessing method that ranks docking poses by binding mode similarity to a reference ligand pose.¹⁰ The IFP scoring method has been shown to outperform docking scoring functions in virtual screening studies^{13,17,26} and was successfully used in recent (crystal) structure-based virtual screening studies to discover new (fragment-like) ligands for GPCRs,^{17,102,103} including H₁R¹⁷ and H₄R.¹⁰³ The PLANTS-IFP and GOLD-IFP docking scoring combinations give satisfactory results in the retrospective virtual screening evaluations against H₃R homology models presented in the current study. The performance of docking-IFP in virtual fragment screening experiments is however significantly lower than the performance of customized FLAP models that are explicitly trained by sets of true fragment-like H₃R actives and inactives. The FLAP method is based on similarity measures between the MIFs of a ligand and a target pocket. Essential molecular interaction features for ligands and proteins are identified and then expressed by a similarity score for each probe used and for probe combinations. FLAP similarity scores are mathematically combined by LDA to derive a score that measures the probability of a ligand to be active or inactive for the screened target. Such estimation by approximated mathematical methods can be used to overcome sampling and scoring issues in structure-based VFS to discriminate active from inactive fragment-like molecules.

The evaluation of structure-based FLAP models by retrospective virtual screening studies can be used to select optimal coordinates of protein–ligand homology models. The ligand 3 bound H₃R homology model yielded a significantly better FLAP model (SB model 1, Figure 10A) than the model that was built based on the ligand 4 bound H₃R model (SB model 2, Figure 10B) in terms of retrospective virtual accuracy (Figure 6, Table 3). Apparently, the first H₃R structure (and its corresponding FLAP pharmacophore) represents a better structural model to accommodate fragment-like H₃R ligands (Figures 6 and 9).

Discovery of Fragment-like H₃R Ligands via a Combined Ligand- and Protein-Based FLAP Approach.

Virtual screening protocols should not only be optimized and validated in retrospective validation studies but also by experimental verification on new data sets that are not considered during model development.³² The integrated ligand- and structure-based FLAP approach applied above in retrospective VFS studies (Figure 4 and Figure 6) were successfully used to identify new H₃R binding fragments from the ZINC database. Eighteen out of 29 tested fragments displayed affinity for H₃R with K_i values ranging from 0.5 to 10 μ M (including fragments 6, 7, and 8 that all have submicromolar affinity for H₃R). The 62% hit rate of our prospective screening study is relatively high compared to previous prospective virtual screening studies for novel ligands of GPCRs¹⁷ or other protein targets.¹⁰⁴ The validated fragments are furthermore relatively small H₃R ligands with high ligand efficiency (Table 4) and are therefore promising new starting points for further ligand optimization. None of the validated hits would have been retrieved by 3D shape-based similarity searches (ROCS) or topological 2D similarity searches (ECFP-4) against FLAP template 5, using previously defined ECFP-4 (Tanimoto \geq 0.40⁹⁶) and ROCS Comboscore (score \geq 1.40)⁹⁷ similarity cutoffs (Supporting Information Figure S10). None of the hits were chemically similar to any of the fragment-like H₃R ligands that were used to train the FLAP models, and only 4 of the 18 experimentally confirmed hits

(compounds 12, 13, 14, and 16) are chemically similar to any known H₃R ligand in the ChEMBL⁹⁵ (i.e., have an ECFP-4 Tanimoto similarity higher than 0.40;⁹⁶ see Table 4). This demonstrates the scaffold hopping potential of FLAP for VFS to enable the identification of chemically novel ligands.

We noticed that many of the experimentally confirmed hits in our prospective virtual screening campaign contain a basic nitrogen separated by 3 or 4 bonds from an aromatic ring (9 out of 18 confirmed hits). However, applying these topological rules as a filter in retrospective virtual screening studies gives significantly lower enrichments in discriminating between known actives and inactives (2–4 fold at 11–15% FP, Supporting Information Table S11) than the enrichments obtained with FLAP LDA-R (23–59 fold at 1% false positive rate, Table 1). Furthermore a high number of 32 171 compounds in the database used for prospective virtual screening contain a basic nitrogen separated by 3 or 4 bonds from an aromatic ring. This further demonstrates that the high prospective virtual screening hit rate obtained in our study are not the result of artificial enrichment.²⁰

Only 2 out of the 18 experimentally validated H₃R hits (6 and 13) had medium affinity for the histamine H₁ receptor (H₁R) (Supporting Information Table S9). These dual H₁R–H₃R ligands share a piperidine ring, a substructure that is commonly found in many known H₁R and H₃R binders.²⁸ On the other hand, ligands 7, 8, and 10 illustrate that also ligands with a piperidine moiety can bind selectively to H₃R. Moreover, none of the validated H₃R hits had affinity for the closely related histamine H₄ receptor (H₄R, Table S9), which is surprising because of the high ligand overlap and binding site similarity between H₃R and H₄R.^{30,105} The experimentally validated fragments are therefore not only promising new ligands of the pharmaceutically relevant histamine H₃ receptor¹⁰⁶ but also interesting new chemical tools to investigate the molecular determinants of ligand selectivity among the histamine receptor family.

CONCLUSION

In this study, the FLAP method was for the first time applied to *in silico* virtual screening for fragment-like molecules. Using the histamine H₃ receptor as a case study, we first validated both ligand- and structure-based models FLAP models in retrospective virtual screening studies. The selection of compounds from both the ChEMBL database and an in-house collection of diverse fragments guaranteed an even distribution of actives and inactives with respect to number of heavy atoms. The in-house fragment collection compensated for the few numbers of inactives that are annotated in the ChEMBL database. LDA-based identification of the same optimal reference template indicated that the ligand-based FLAP models were data set independent. Cumulative MIF analysis of ligand-based FLAP models enabled the definition of conserved pharmacophoric properties of H₃R ligands that are absent in molecules that do not have affinity for H₃R. Essential pharmacophore features defined in ligand-based FLAP models were complementary to the H₃R features derived from structure-based FLAP models, illustrating the use of FLAP modeling to derive structural information of protein–ligand complexes. Ligand-based and protein-based FLAP models were significantly better than other ligand- and structure-based virtual screening methods in retrospective virtual screening studies. The lessons learned from retrospective studies were used for a prospective VS study of 156 090 fragment-like commercially available compounds. A

set of 29 novel compounds was selected by a combined ligand- and structure-based FLAP approach, of which 18 were confirmed as H₃R ligands with affinities ranging from 0.5 to 10 μ M. Our studies demonstrate that customized VFS strategies based on training sets of true active and inactive fragment-like molecules are required to overcome the challenges of *in silico* fragment screening.

■ ASSOCIATED CONTENT

■ Supporting Information

Additional analyses of ligand databases and the retrospective and prospective virtual screening studies, H₁R, H₃R, and H₄R radioligand displacement curves, OpenEye Filter configuration file, supplier information, and LCMS and NMR purity for experimentally validated compounds. This material is available free of charge via the Internet at <http://pubs.acs.org>.

■ AUTHOR INFORMATION

Corresponding Author

*Tel.: +31(0)20-5987553. Fax: +31(0)20-5987610. E-mail: c.de.graaf@vu.nl.

Notes

The authors declare no competing financial interest.

■ ACKNOWLEDGMENTS

The authors thank Herman D. Lim for technical assistance with the H₁R, H₃R, and H₄R binding assays and the LCMS analyses. This research was financially supported by The Netherlands Organization for Scientific Research (NWO) through a VENI grant (Grant 700.59.408 to C.d.G.), by TI-Pharma through Grant D1-105 (GPCR Forum to E.P.I. and A.J.K.), and by Molecular Discovery Ltd. (215 Marsh Road, HA5 SNE, Pinner, Middlesex, United Kingdom to F.S.).

■ ABBREVIATIONS

FBDD, fragment-based drug discovery; VFS, virtual fragment screening; FLAP, fingerprints for ligands and proteins; GPCR, G-protein coupled receptor; H₁R, histamine H₁ receptor; H₃R, histamine H₃ receptor; H₄R, histamine H₄ receptor; IFP, interaction fingerprint; LDA, linear discriminant analysis; MD, molecular dynamics; MIFs, molecular interaction fields; ROC, receiver operating characteristic; SAR, structure–activity relationship; VFS, virtual fragment screening

■ REFERENCES

- (1) Verheij, M. H. P.; de Graaf, C.; de Kloe, G. E.; Nijmeijer, S.; Vischer, H. F.; Smits, R. A.; Zuiderveld, O. P.; Hulscher, S.; Silvestri, L.; Thompson, A. J.; van Muijlwijk-Koezen, J. E.; Lummis, S. C. R.; Leurs, R.; de Esch, I. J. P. Fragment library screening reveals remarkable similarities between the G protein-coupled receptor histamine H(4) and the ion channel serotonin 5-HT(3A). *Bioorg. Med. Chem. Lett.* **2011**, *21*, 5460–5464.
- (2) Congreve, M.; Carr, R.; Murray, C.; Jhoti, H. A 'rule of three' for fragment-based lead discovery? *Drug Discovery Today* **2003**, *8*, 876–7.
- (3) Murray, C. W.; Verdonk, M. L.; Rees, D. C. Experiences in fragment-based drug discovery. *Trends Pharmacol. Sci.* **2012**, *33*, 224–32.
- (4) de Graaf, C.; Vischer, H. F.; de Kloe, G. E.; Kooistra, A. J.; Nijmeijer, S.; Kuijer, M.; Verheij, M. H. P.; England, P.; van Muijlwijk-Koezen, J. E.; Leurs, R.; de Esch, I. J. P. Small and colourful stones make beautiful mosaics: Fragment-Based Chemogenomics. *Drug Discovery Today* **2012**, DOI: <http://dx.doi.org/10.1016/j.drudis.2012>.
- (5) de Kloe, G. E.; Bailey, D.; Leurs, R.; de Esch, I. J. P. Transforming fragments into candidates: small becomes big in medicinal chemistry. *Drug Discovery Today* **2009**, *14*, 630–646.
- (6) Schultes, S.; De Graaf, C.; Haaksma, E. J.; De Esch, I. J. P.; Leurs, R.; Kramer, O. Ligand efficiency as a guide in fragment hit selection and optimization. *Drug Discovery Today: Technol.* **2010**, *7*, 153–162.
- (7) Congreve, M.; Chessari, G.; Tisi, D.; Woodhead, A. J. Recent developments in fragment-based drug discovery. *J. Med. Chem.* **2008**, *51*, 3661–80.
- (8) Yuriev, E.; Agostino, M.; Ramsland, P. A. Challenges and advances in computational docking: 2009 in review. *J. Molec. Recog.* **2011**, *24*, 149–164.
- (9) Reymond, J.-L.; van Deursen, R.; Blum, L. C.; Ruddigkeit, L. Chemical space as a source for new drugs. *MedChemComm* **2010**, *1*, 30–38.
- (10) Moitessier, N.; Englebienne, P.; Lee, D.; Lawandi, J.; Corbeil, C. R. Towards the development of universal, fast and highly accurate docking/scoring methods: a long way to go. *Br. J. Pharmacol.* **2008**, *153*, S7–S26.
- (11) Wijtmans, M.; de Graaf, C.; de Kloe, G.; Istyastono, E. P.; Smit, J.; Lim, H.; Boonnak, R.; Nijmeijer, S.; Smits, R. A.; Jongejan, A.; Zuiderveld, O.; de Esch, I. J. P.; Leurs, R. Triazole Ligands Reveal Distinct Molecular Features That Induce Histamine H(4) Receptor Affinity and Subtly Govern H(4)/H(3) Subtype Selectivity. *J. Med. Chem.* **2011**, *54*, 1693–1703.
- (12) Loving, K.; Alberts, I.; Sherman, W. Computational Approaches for Fragment-Based and De Novo Design. *Curr. Top. Med. Chem.* **2010**, *10*, 14–32.
- (13) Marcou, G.; Rognan, D. Optimizing fragment and scaffold docking by use of molecular interaction fingerprints. *J. Chem. Inf. Model.* **2007**, *47*, 195–207.
- (14) Crisman, T. J.; Bender, A.; Milik, M.; Jenkins, J. L.; Scheiber, J.; Sukuru, S. C. K.; Fejzo, J.; Hommel, U.; Davies, J. W.; Glick, M. "Virtual fragment linking": an approach to identify potent binders from low affinity fragment hits. *J. Med. Chem.* **2008**, *51*, 2481–2491.
- (15) Villar, H. O.; Hansen, M. R. Computational techniques in fragment based drug discovery. *Curr. Top. Med. Chem.* **2007**, *7*, 1509–1513.
- (16) Chen, Y.; Shoichet, B. K. Molecular docking and ligand specificity in fragment-based inhibitor discovery. *Nat. Chem. Biol.* **2009**, *5*, 358–364.
- (17) de Graaf, C.; Kooistra, A. J.; Vischer, H. F.; Katritch, V.; Kuijer, M.; Shiroishi, M.; Iwata, S.; Shimamura, T.; Stevens, R. C.; de Esch, I. J. P.; Leurs, R. Crystal Structure-Based Virtual Screening for Fragment-like Ligands of the Human Histamine H(1) Receptor. *J. Med. Chem.* **2011**, *54*, 8195–8206.
- (18) de Graaf, C.; Rognan, D. Customizing G Protein-Coupled Receptor Models for Structure-Based Virtual Screening. *Curr. Pharm. Des.* **2009**, *15*, 4026–4048.
- (19) Katritch, V.; Cherezov, V.; Stevens, R. C. Diversity and modularity of G protein-coupled receptor structures. *Trends Pharmacol. Sci.* **2012**, *33*, 17–27.
- (20) Verdonk, M. L.; Berdini, V.; Hartshorn, M. J.; Mooij, W. T. M.; Murray, C. W.; Taylor, R. D.; Watson, P. Virtual screening using protein-ligand docking: Avoiding artificial enrichment. *J. Chem. Inf. Comput. Sci.* **2004**, *44*, 793–806.
- (21) Gleeson, M. P.; Gleeson, D. QM/MM As a Tool in Fragment Based Drug Discovery. A Cross-Docking, Rescoring Study of Kinase Inhibitors. *J. Chem. Inf. Model.* **2009**, *49*, 1437–1448.
- (22) Verdonk, M. L.; Giangreco, I.; Hall, R. J.; Korb, O.; Mortenson, P. N.; Murray, C. W. Docking Performance of Fragments and Drug like Compounds. *J. Med. Chem.* **2011**, *54*, 5422–5431.
- (23) Holliday, J. D.; Salim, N.; Whittle, M.; Willett, P. Analysis and display of the size dependence of chemical similarity coefficients. *J. Chem. Inf. Comput. Sci.* **2003**, *43*, 819–28.
- (24) Flower, D. R. On the properties of bit string-based measures of chemical similarity. *J. Chem. Inf. Comput. Sci.* **1998**, *38*, 379–386.
- (25) Huang, X.; Lai, J.; Jennings, S. F. Maximum common subgraph: some upper bound and lower bound results. *BMC Bioinf.* **2006**, *7*.

- (26) de Graaf, C.; Rognan, D. Selective Structure-Based Virtual Screening for Full and Partial Agonists of the beta 2 Adrenergic Receptor. *J. Med. Chem.* **2008**, *51*, 4978–4985.
- (27) Olah, M.; Rad, L.; Ostopovici, L.; Bora, A.; Hadaruga, N.; Hadaruga, D.; Moldovan, R.; Fulas, A.; Mracec, M.; Oprea, T. I. WOMBAT and WOMBAT-PK: Bioactivity Databases for Lead and Drug Discovery. In *Chemical Biology: From Small Molecules to Systems Biology and Drug Design*; Wiley-VCH Verlag GmbH: Weinheim, Germany, 2008; pp 1–3.
- (28) Gaulton, A.; Bellis, L. J.; Bento, A. P.; Chambers, J.; Davies, M.; Hersey, A.; Light, Y.; McGlinchey, S.; Michalovich, D.; Al-Lazikani, B.; Overington, J. P. ChEMBL: a large-scale bioactivity database for drug discovery. *Nucl. Acids Res.* **2012**, *40* (D1), D1100–D1107.
- (29) Knox, C.; Law, V.; Jewison, T.; Liu, P.; Ly, S.; Frolkis, A.; Pon, A.; Banco, K.; Mak, C.; Neveu, V.; Djoumbou, Y.; Eisner, R.; Guo, A. C.; Wishart, D. S. DrugBank 3.0: a comprehensive resource for 'omics' research on drugs. *Nucl. Acids Res.* **2011**, *39* (Database issue), D1035–D1041.
- (30) Chen, X.; Lin, Y.; Gilson, M. K. The binding database: Overview and user's guide. *Biopolymers* **2002**, *61* (2), 127–141.
- (31) Nicholls, A. What do we know and when do we know it? *J. Comput.-Aided Molec. Des.* **2008**, *22*, 239–255.
- (32) Scior, T.; Bender, A.; Tresadern, G.; Medina-Franco, J. L.; Martínez-Mayorga, K.; Langer, T.; Cuanalo-Contreras, K.; Agrafiotis, D. K. Recognizing Pitfalls in Virtual Screening: A Critical Review. *J. Chem. Inf. Model.* **2012**, *52*, 867–881.
- (33) Leurs, R.; Bakker, R. A.; Timmerman, H.; de Esch, I. J. The histamine H3 receptor: from gene cloning to H3 receptor drugs. *Nat. Rev. Drug. Discov.* **2005**, *4*, 107–120.
- (34) Berlin, M.; Boyce, C. W.; Ruiz, M. d. L. Histamine H(3) Receptor as a Drug Discovery Target. *J. Med. Chem.* **2011**, *54*, 26–53.
- (35) Celanire, S.; Wijtmans, M.; Talaga, P.; Leurs, R.; de Esch, I. J. P. Histamine H-3 receptor antagonists reach out for the clinic. *Drug Discovery Today* **2005**, *10*, 1613–1627.
- (36) Baroni, M.; Cruciani, G.; Sciabola, S.; Perruccio, F.; Mason, J. S. A common reference framework for analyzing/comparing proteins and ligands. Fingerprints for ligands and proteins (FLAP): Theory and application. *J. Chem. Inf. Model.* **2007**, *47*, 279–294.
- (37) Goodford, P. J. A computational procedure for determining energetically favorable binding-sites on biologically important macromolecules. *J. Med. Chem.* **1985**, *28*, 849–857.
- (38) Brincat, J. P.; Carosati, E.; Sabatini, S.; Manfroni, G.; Fravolini, A.; Raygada, J. L.; Pate, D.; Kaatz, G. W.; Cruciani, G. Discovery of Novel Inhibitors of the NorA Multidrug Transporter of *Staphylococcus aureus*. *J. Med. Chem.* **2011**, *54*, 354–365.
- (39) Cross, S.; Baroni, M.; Carosati, E.; Benedetti, P.; Clementi, S. FLAP: GRID Molecular Interaction Fields in Virtual Screening. Validation using the DUD Data Set. *J. Chem. Inf. Model.* **2010**, *50*, 1442–1450.
- (40) Carosati, E.; Mannhold, R.; Wahl, P.; Hansen, J. B.; Fremming, T.; Zamora, I.; Cianchetta, G.; Baroni, M. Virtual screening for novel openers of pancreatic K-ATP channels. *J. Med. Chem.* **2007**, *50*, 2117–2126.
- (41) Rogers, D.; Hahn, M. Extended-Connectivity Fingerprints. *J. Chem. Inf. Model.* **2010**, *50*, 742–754.
- (42) Grant, J. A.; Gallardo, M. A.; Pickup, B. T. A fast method of molecular shape comparison: A simple application of a Gaussian description of molecular shape. *J. Comput. Chem.* **1996**, *17*, 1653–1666.
- (43) Korb, O.; Stützel, T.; Exner, T. E. An ant colony optimization approach to flexible protein-ligand docking. *Swarm Intell.* **2007**, *1*, 115–134.
- (44) Jones, G.; Willett, P.; Glen, R. C.; Leach, A. R.; Taylor, R. Development and Validation of a Genetic Algorithm for Flexible Docking. *J. Mol. Biol.* **1997**, *267*, 727–748.
- (45) Fisher, R. A. The Use of Multiple Measurements in Taxonomic Problems. *Ann. Eugenics* **1936**, *7*, 179–188.
- (46) McLachlan, G. J. *Discriminant Analysis and Statistical Pattern Recognition*; Wiley Series in Probability and Statistics; Wiley-Interscience: New York, 2004.
- (47) Sirci, F.; Goracci, L.; Rodríguez, D.; van Muijlwijk-Koezen, J.; Gutiérrez-de-Terán, H.; Mannhold, R. Ligand-, structure- and pharmacophore-based molecular fingerprints: a case study on adenosine A1, A2A, A2B, and A3 receptor antagonists. *J. Comput.-Aided Molec. Des.* **2012**, DOI: 10.1007/s10822-012-9612-8.
- (48) Gasteiger, J.; Teckentrup, A.; Terfloth, L.; Spycher, S. Neural networks as data mining tools in drug design. *J. Phys. Org. Chem.* **2003**, *16*, 232–245.
- (49) Milletti, F.; Storch, L.; Sforna, G.; Cruciani, G. New and original pK(a) prediction method using grid molecular interaction fields. *J. Chem. Inf. Model.* **2007**, *47*, 2172–2181.
- (50) FILTER, version 2.1.1; OpenEye Scientific Software: Santa Fe, NM, 2011; <http://www.eyesopen.com/filter>.
- (51) Sciabola, S.; Stanton, R. V.; Mills, J. E.; Flocco, M. M.; Baroni, M.; Cruciani, G.; Perruccio, F.; Mason, J. S. High-Throughput Virtual Screening of Proteins Using GRID Molecular Interaction Fields. *J. Chem. Inf. Model.* **2010**, *50*, 155–169.
- (52) Ioan, P.; Ciogli, A.; Sirci, F.; Budriesi, R.; Cosimelli, B.; Pierini, M.; Severi, E.; Chiarini, A.; Cruciani, G.; Gasparrini, F.; Spinelli, D.; Carosati, E. Absolute configuration and biological profile of two thiazinooxadiazol-3-ones with L-type calcium channel activity: a study of the structural effects. *Org. Biomol. Chem.* **2012**, *10*, 8994–9003.
- (53) Shimamura, T.; Shiroishi, M.; Weyand, S.; Tsujimoto, H.; Winter, G.; Katritch, V.; Abagyan, R.; Cherezov, V.; Liu, W.; Han, G. W.; Kobayashi, T.; Stevens, R. C.; Iwata, S. Structure of the human histamine H(1) receptor complex with doxepin. *Nature* **2011**, *475*, 65–70.
- (54) Shi, L.; Javitch, J. A. The binding site of aminergic G protein-coupled receptors: The transmembrane segments and second extracellular loop. *Annu. Rev. Pharmacol. Toxicol.* **2002**, *42*, 437–467.
- (55) Ohta, K.; Hayashi, H.; Mizuguchi, H.; Kagamiyama, H.; Fujimoto, K.; Fukui, H. Site-directed mutagenesis of the histamine H1 receptor - Role of the aspartic acid (107), asparagine (198) and threonine (194). *Biochem. Biophys. Res. Commun.* **1994**, *203*, 1096–1101.
- (56) Gantz, I.; Delvalle, J.; Wang, L. D.; Tashiro, T.; Munzert, G.; Guo, Y. J.; Konda, Y.; Yamada, T. Molecular basis for the interaction of histamine with the histamine H2 receptor. *J. Biol. Chem.* **1992**, *267*, 20840–20843.
- (57) Jongejans, A.; Lim, H. D.; Smits, R. A.; de Esch, I. J. P.; Haaksma, E.; Leurs, R. Delineation of agonist binding to the human histamine H-4 receptor using mutational analysis, homology modeling, and ab initio calculations. *J. Chem. Inf. Model.* **2008**, *48*, 1455–1463.
- (58) Shin, N.; Coates, E.; Murgolo, N. J.; Morse, K. L.; Bayne, M.; Strader, C. D.; Monsma, F. J. Molecular Modeling and site-specific mutagenesis of the histamine-binding site of the histamine H-4 receptor. *Mol. Pharmacol.* **2002**, *62*, 38–47.
- (59) Pipeline Pilot, version 6.1.5; Accelrys: San Diego, CA, 2008; <http://accelrys.com/products/pipeline-pilot/>.
- (60) Bostrom, J.; Greenwood, J. R.; Gottfries, J. Assessing the performance of OMEGA with respect to retrieving bioactive conformations. *J. Molec. Graph. Modell.* **2003**, *21*, 449–462.
- (61) ROCs, version 2.3.1; OpenEye Scientific Software: Santa Fe, NM, 2011; <http://www.eyesopen.com/rocs>.
- (62) Fulekar, M. H. *Bioinformatics: Application in Life and Environmental Sciences*; Springer: Dordrecht, The Netherlands, 2009; p 110.
- (63) Jain, A. N.; Nicholls, A. Recommendations for evaluation of computational methods. *J. Comput.-Aided Molec. Des.* **2008**, *22*, 133–139.
- (64) Istyastono, E. P.; Nijmeijer, S.; Lim, H. D.; van de Stolpe, A.; Roumen, L.; Kooistra, A. J.; Vischer, H. F.; de Esch, S. J. P.; Leurs, R.; de Graaf, C. Molecular Determinants of Ligand Binding Modes in the Histamine H(4) Receptor: Linking Ligand-Based Three-Dimensional Quantitative Structure-Activity Relationship (3D-QSAR) Models to in

Silico Guided Receptor Mutagenesis Studies. *J. Med. Chem.* **2011**, *54*, 8136–8147.

(65) Uveges, A. J.; Kowal, D.; Zhang, Y. X.; Spangler, T. B.; Dunlop, J.; Semus, S.; Jones, P. G. The role of transmembrane helix 5 in agonist binding to the human H3 receptor. *J. Pharmacol. Exp. Ther.* **2002**, *301*, 451–458.

(66) Case, D. A.; Darden, T. A.; Cheatham, T. E.; Simmerling, C. L.; Wang, L.; Duke, R. E.; Luo, R.; Walker, R. C.; Zhang, W.; Merz, K. M.; Roberts, B.; Wang, B.; Hayik, S.; Roitberg, A. G.; Seabra, I.; Kolossvai, K. F.; Wong, F.; Paesani, J.; Vanicek, J.; Liu, X.; Wu, S. R.; Brozell, T.; Steinbrecher, H.; Gohlke, Q.; Cai, X.; Ye, J.; Wang, M. J.; Hsieh, G.; Cui, D. R.; Roe, D. H.; Mathews, M. G.; Seetin, C.; Sagui, V.; Babin, T.; Luchko, S.; Gusarov, A.; Kovalenko, P. A.; Kollman. *AMBER 11*; University of California, San Francisco, 2010.

(67) Wang, J.; Wang, W.; Kollman, P. Antechamber, an accessory software package for molecular mechanical calculations. *J. Comput. Chem.* **2005**, *25*, 1157–1174.

(68) Urizar, E.; Claeysen, S.; Deupi, X.; Govaerts, C.; Costagliola, S.; Vassart, G.; Pardo, L. An activation switch in the rhodopsin family of G protein-coupled receptors - The thyrotropin receptor. *J. Biol. Chem.* **2005**, *280*, 17135–17141.

(69) Jarvis, R. A.; Patrick, E. A. Clustering Using a Similarity Measure Based on Shared Near Neighbors. *IEEE Trans. Comput.* **1973**, *C-22*, 1025–1034.

(70) Cheng, Y.; Prusoff, W. H. Relationship between the inhibition constant (K_i) and the concentration of inhibitor which causes 50% inhibition (I_{50}) of an enzymatic reaction. *Biochem. Pharma.* **1973**, *22*, 3099–108.

(71) Govoni, M.; Lim, H. D.; El-Atmioui, D.; Menge, W.; Timmerman, H.; Bakker, R. A.; Leurs, R.; De Esch, I. J. P. A chemical switch for the modulation of the functional activity of higher homologues of histamine on the human histamine H-3 receptor: Effect of various substitutions at the primary amino function. *J. Med. Chem.* **2006**, *49*, 2549–2557.

(72) Tawa, G. J.; Baber, J. C.; Humblet, C. Computation of 3D queries for ROCS based virtual screens. *J. Comput.-Aided Molec. Des.* **2009**, *23*, 853–868.

(73) Swann, S. L.; Brown, S. P.; Muchmore, S. W.; Patel, H.; Merta, P.; Locklear, J.; Hajduk, P. J. A Unified, Probabilistic Framework for Structure- and Ligand-Based Virtual Screening. *J. Med. Chem.* **2011**, *54*, 1223–1232.

(74) Krueger, D. M.; Evers, A. Comparison of Structure- and Ligand-Based Virtual Screening Protocols Considering Hit List Complementarity and Enrichment Factors. *ChemMedChem* **2010**, *5*, 148–158.

(75) Nettles, J. H.; Jenkins, J. L.; Bender, A.; Deng, Z.; Davies, J. W.; Glick, M. Bridging chemical and biological space: “Target fishing” using 2D and 3D molecular descriptors. *J. Med. Chem.* **2006**, *49*, 6802–6810.

(76) Yeap, S. K.; Walley, R. J.; Snarey, M.; van Hoorn, W. P.; Mason, J. S. Designing compound subsets: Comparison of random and rational approaches using statistical simulation. *J. Chem. Inf. Model.* **2007**, *47*, 2149–2158.

(77) Kogej, T.; Engkvist, O.; Blomberg, N.; Muresan, S. Multi-fingerprint based similarity searches for targeted class compound selection. *J. Chem. Inf. Model.* **2006**, *46*, 1201–1213.

(78) Oellien, F.; Cramer, J.; Beyer, C.; Ihlenfeldt, W.-D.; Selzer, P. M. The impact of tautomer forms on pharmacophore-based virtual screening. *J. Chem. Inf. Model.* **2006**, *46*, 2342–2354.

(79) Park, M.-S.; Gao, C.; Stern, H. A. Estimating binding affinities by docking/scoring methods using variable protonation states. *Proteins-Struct. Funct. Bioinf.* **2011**, *79*, 304–314.

(80) Greenwood, J. R.; Calkins, D.; Sullivan, A. P.; Shelley, J. C. Towards the comprehensive, rapid, and accurate prediction of the favorable tautomeric states of drug-like molecules in aqueous solution. *J. Comput.-Aided Molec. Des.* **2010**, *24*, 591–604.

(81) Martin, Y. C. Lets not forget tautomers. *J. Comput.-Aided Molec. Des.* **2009**, *23*, 693–704.

(82) Milletti, F.; Storch, L.; Sforza, G.; Cross, S.; Cruciani, G. Tautomer Enumeration and Stability Prediction for Virtual Screening on Large Chemical Databases. *J. Chem. Inf. Model.* **2009**, *49*, 68–75.

(83) ten Brink, T.; Exner, T. E. pK(a) based protonation states and microspecies for protein-ligand docking. *J. Comput.-Aided Molec. Des.* **2010**, *24*, 935–942.

(84) Milletti, F.; Vulpetti, A. Tautomer Preference in PDB Complexes and its Impact on Structure-Based Drug Discovery. *J. Chem. Inf. Model.* **2010**, *50*, 1062–1074.

(85) Polgar, T.; Magyar, C.; Simon, I.; Keserue, G. M. Impact of ligand protonation on virtual screening against ss-secretase (BACE1). *J. Chem. Inf. Model.* **2007**, *47*, 2366–2373.

(86) Kitbunnadaj, R.; Hashimoto, T.; Poli, E.; Zuiderveld, O. P.; Menozzi, A.; Hidaka, R.; de Esch, I. J. P.; Bakker, R. A.; Menge, W.; Yamatodani, A.; Coruzzi, G.; Timmerman, H.; Leurs, R. N-substituted piperidinyl alkyl imidazoles: Discovery of methimepip as a potent and selective histamine H-3 receptor agonist. *J. Med. Chem.* **2005**, *48*, 2100–2107.

(87) De Esch, I. J. P.; Mills, J. E. J.; Perkins, T. D. J.; Romeo, G.; Hoffmann, M.; Wieland, K.; Leurs, R.; Menge, W.; Nederkoorn, P. H. J.; Dean, P. M.; Timmerman, H. Development of a pharmacophore model for histamine H-3 receptor antagonists, using the newly developed molecular modeling program SLATE. *J. Med. Chem.* **2001**, *44*, 1666–1674.

(88) Mills, J. E. J.; de Esch, I. J. P.; Perkins, T. D. J.; Dean, P. M. SLATE: A method for the superposition of flexible ligands. *J. Comput.-Aided Molec. Des.* **2001**, *15*, 81–96.

(89) <http://zinc.docking.org/>. Accessed April 2011.

(90) Irwin, J. J.; Shoichet, B. K. ZINC - A free database of commercially available compounds for virtual screening. *J. Chem. Inf. Model.* **2005**, *45*, 177–182.

(91) Oprea, T. I. Property distribution of drug-related chemical databases. *J. Comput.-Aided Molec. Des.* **2000**, *14*, 251–264.

(92) Rishton, G. M. Reactive compounds and in vitro false positives in HTS. *Drug Discovery Today* **1997**, *2*, 382–384.

(93) Olah, M. M.; Bologa, C. G.; Oprea, T. I. Strategies for compound selection. *Curr. Drug Discovery Technol.* **2004**, *1*, 211–20.

(94) Congreve, M.; Carr, R.; Murray, C.; Jhoti, H. A rule of three for fragment-based lead discovery? *Drug Discovery Today* **2003**, *8*, 876–877.

(95) <https://www.ebi.ac.uk/chembl/>. Accessed April 2011.

(96) Wawer, M.; Bajorath, J. Similarity-Potency Trees: A Method to Search for SAR Information in Compound Data Sets and Derive SAR Rules. *J. Chem. Inf. Model.* **2010**, *50*, 1395–1409.

(97) Blum, L. C.; van Deursen, R.; Reymond, J.-L. Visualisation and subsets of the chemical universe database GDB-13 for virtual screening. *J. Comput.-Aided Molec. Des.* **2011**, *25*, 637–647.

(98) Bender, A.; Jenkins, J. L.; Scheiber, J.; Sukuru, S. C. K.; Glick, M.; Davies, J. W. How Similar Are Similarity Searching Methods? A Principal Component Analysis of Molecular Descriptor Space. *J. Chem. Inf. Model.* **2009**, *49*, 108–119.

(99) Duan, J.; Dixon, S. L.; Lowrie, J. F.; Sherman, W. Analysis and comparison of 2D fingerprints: Insights into database screening performance using eight fingerprint methods. *J. Molec. Graph. Modell.* **2010**, *29*, 157–170.

(100) Sousa, S. F.; Fernandes, P. A.; Ramos, M. J. Protein-ligand docking: Current status and future challenges. *Proteins-Struct. Funct. Bioinf.* **2006**, *65*, 15–26.

(101) Lee, J.; Seok, C. A statistical rescoring scheme for protein-ligand docking: Consideration of entropic effect. *Proteins-Struct. Funct. Bioinf.* **2008**, *70*, 1074–1083.

(102) de Graaf, C.; Rein, C.; Piwnicka, D.; Giordanetto, F.; Rognan, D. Structure-based discovery of allosteric modulators of two related class B G-protein-coupled receptors. *ChemMedChem* **2011**, *6*, 2159–69.

(103) Istyastono, E. P. *Computational Studies of Histamine H4 Receptor-Ligand Interactions*. Ph.D. thesis, VU University Amsterdam, Amsterdam, 2012.

(104) Rognan, D. Docking Methods for Virtual Screening: Principles and Recent Advances. In *Virtual Screening*; Wiley-VCH Verlag GmbH & Co. KGaA: Weinheim, Germany, 2011; pp 153–176.

(105) Kim, S.-K.; Fristrup, P.; Abrol, R.; Goddard, W. A. III. Structure-Based Prediction of Subtype Selectivity of Histamine H(3) Receptor Selective Antagonists in Clinical Trials. *J. Chem. Inf. Model.* **2011**, *51*, 3262–3274.

(106) Kuhne, S.; Wijtmans, M.; Lim, H. D.; Leurs, R.; de Esch, I. J. P. Several down, a few to go: histamine H(3) receptor ligands making the final push towards the market? *Expert Opin. Invest. Drugs* **2011**, *20*, 1629–1648.

(107) Istyastono, E. P.; de Graaf, C.; de Esch, I. J. P.; Leurs, R. Molecular Determinants of Selective Agonist and Antagonist Binding to the Histamine H(4) Receptor. *Curr. Top. Med. Chem.* **2011**, *11*, 661–679.

(108) Lim, H. D.; van Rijn, R. M.; Ling, P.; Bakker, R. A.; Thurmond, R. L.; Leurs, R. Evaluation of histamine H-1-, H-2-, and H-3-receptor ligands at the human histamine H-4 receptor: Identification of 4-methylhistamine as the first potent and selective H-4 receptor agonist. *J. Pharmacol. Exp. Ther.* **2005**, *314*, 1310–1321.